

# Northumbria Research Link

Citation: Cartmell, Alan, Munoz, Jose, Briggs, Jonathon, Ndeh, Didier, Lowe, Elisabeth, Baslé, Arnaud, Terrapon, Nicolas, Stott, Katherine, Heunis, Tiaan, Gray, Joe, Yu, Li, Dupree, Paul, Fernandes, Pearl, Shah, Sayali, Williams, Spencer, Labourel, Aurore, Trost, Matthias, Henrissat, Bernard and Gilbert, Harry (2018) A surface endogalactanase in *Bacteroides thetaiotaomicron* confers keystone status for arabinogalactan degradation. *Nature Microbiology*, 3 (11). pp. 1314-1326. ISSN 2058-5276

Published by: Nature Publishing

URL: <https://doi.org/10.1038/s41564-018-0258-8> <<https://doi.org/10.1038/s41564-018-0258-8>>

This version was downloaded from Northumbria Research Link:  
<http://nrl.northumbria.ac.uk/id/eprint/37753/>

Northumbria University has developed Northumbria Research Link (NRL) to enable users to access the University's research output. Copyright © and moral rights for items on NRL are retained by the individual author(s) and/or other copyright owners. Single copies of full items can be reproduced, displayed or performed, and given to third parties in any format or medium for personal research or study, educational, or not-for-profit purposes without prior permission or charge, provided the authors, title and full bibliographic details are given, as well as a hyperlink and/or URL to the original metadata page. The content must not be changed in any way. Full items must not be sold commercially in any format or medium without formal permission of the copyright holder. The full policy is available online: <http://nrl.northumbria.ac.uk/policies.html>

This document may differ from the final, published version of the research and has been made available online in accordance with publisher policies. To read and/or cite from the published version of the research, please visit the publisher's website (a subscription may be required.)

1 **Engineering a surface endogalactanase into *Bacteroides thetaiotaomicron* confers**  
2 **keystone status for arabinogalactan degradation**

3  
4 Alan Cartmell<sup>1¶</sup>, Jose Muñoz-Muñoz<sup>1,2¶</sup>, Jonathon Briggs<sup>1¶</sup>, Didier A. Ndeh<sup>1¶</sup>, Elisabeth C.  
5 Lowe<sup>1</sup>, Arnaud Baslé<sup>1</sup>, Nicolas Terrapon<sup>3</sup>, Katherine Stott<sup>4</sup>, Tiaan Heunis<sup>1</sup>, Joe Gray<sup>1</sup>, Li Yu<sup>4</sup>,  
6 Paul Dupree<sup>4</sup>, Pearl Z. Fernandes<sup>5</sup>, Sayali Shah<sup>5</sup>, Spencer J. Williams<sup>5</sup>, Aurore Labourel<sup>1</sup>,  
7 Matthias Trost<sup>1</sup>, Bernard Henrissat<sup>3,6,7</sup> and Harry J. Gilbert<sup>1,\*</sup>

8  
9 <sup>1</sup>*Institute for Cell and Molecular Biosciences, Newcastle University, Newcastle upon Tyne*  
10 *NE2 4HH, U.K.*

11  
12 <sup>2</sup>*Department of Applied Sciences, Faculty of Health and Life Sciences,*  
13 *Northumbria University, Newcastle upon Tyne, NE1 8ST, UK.*

14  
15 <sup>3</sup>*Architecture et Fonction des Macromolécules Biologiques, Centre National de la Recherche*  
16 *Scientifique (CNRS), Aix-Marseille University, F-13288 Marseille, France*

17  
18 <sup>4</sup>*Department of Biochemistry, University of Cambridge, Cambridge, CB2 1QW, U.K.*

19  
20 <sup>5</sup>*School of Chemistry and Bio21 Molecular Science and Biotechnology Institute,*  
21 *University of Melbourne, Parkville, Victoria 3010, Australia*

22  
23 <sup>6</sup>*INRA, USC 1408 AFMB, F-13288 Marseille, France*

24  
25 <sup>7</sup>*Department of Biological Sciences, King Abdulaziz University, Jeddah, Saudi Arabia*

26  
27 ¶These authors contributed equally.

28  
29 \*To whom correspondence should be addressed: Harry J. Gilbert (harry.gilbert@ncl.ac.uk),  
30  
31  
32  
33  
34  
35  
36  
37  
38  
39

40

41

42 **Abstract**

43 **Glycans are major nutrients for the human gut microbiota (HGM). Arabinogalactan**  
44 **proteins (AGPs) comprise a heterogenous group of plant glycans in which a  $\beta$ 1,3-**  
45 **galactan backbone and  $\beta$ 1,6-galactan side chains are conserved. Diversity is provided**  
46 **by the variable nature of the sugars that decorate the galactans. The mechanisms by**  
47 **which nutritionally relevant AGPs are degraded in the HGM are poorly understood.**  
48 **Here we explore how the HGM organism *Bacteroides thetaiotaomicron* metabolises**  
49 **AGPs. We propose a sequential degradative model in which exo-acting glycoside**  
50 **hydrolase (GH) family 43  $\beta$ 1,3-galactanases release the side chains. These**  
51 **oligosaccharide side chains are depolymerized by the synergistic action of exo-acting**  
52 **enzymes in which catalytic interactions are dependent on whether degradation is**  
53 **initiated by a lyase or GH. We identified two GHs that establish two previously**  
54 **undiscovered GH families. The crystal structures of the exo- $\beta$ 1,3-galactanases**  
55 **identified a key specificity determinant and departure from the canonical catalytic**  
56 **apparatus of GH43 enzymes. Growth studies of *Bacteroidetes* spp. on complex AGP**  
57 **revealed three keystone organisms that facilitated utilisation of the glycan by 17**  
58 **recipient bacteria, which included *B. thetaiotaomicron*. A surface endo- $\beta$ 1,3-**  
59 **galactanase, when engineered into *B. thetaiotaomicron*, enabled the bacterium to**  
60 **utilise complex AGPs and act as a keystone organism.**

61

62

63 The human gut microbiota (HGM) contributes to the physiology and health of its host<sup>1</sup>.  
64 Glycans, the major nutrients for the HGM, are degraded primarily by *Bacteroides* species  
65 within this ecosystem<sup>2-4</sup>. Understanding glycan utilisation in the HGM underpins prebiotic  
66 and probiotic strategies that promote human health. Glycan degradation is mediated by  
67 carbohydrate active enzymes (CAZymes), primarily glycoside hydrolases (GHs) and  
68 polysaccharide lyases (PLs)<sup>5</sup>, which are grouped into sequence-based families on the CAZy  
69 database (<http://www.cazy.org/>)<sup>6</sup>. Although there is structural and catalytic conservation  
70 within families, substrate specificity may vary<sup>7</sup>. Genes encoding glycan degrading systems  
71 are up-regulated by the target carbohydrate and are physically linked within polysaccharide  
72 utilisation loci (PULs)<sup>8,9</sup>. Glycan depolymerisation is generally initiated by bacterial surface  
73 endo-acting GHs/PLs, and the oligosaccharides generated imported into the periplasm and  
74 further metabolised<sup>9-11</sup>.

75

76 A ubiquitous component of the human diet are arabinogalactan proteins (AGPs). These  
77 proteoglycans are in every taxonomic plant group<sup>12</sup>, with high concentrations in processed  
78 foods such as red wine and instant coffee<sup>13,14</sup>. Gum Arabic AGP (GA-AGP) is widely used in  
79 the food industry to improve biophysical properties of many products<sup>15</sup>. AGPs comprise a  
80  $\beta$ 1,3-galactan backbone with  $\beta$ 1,6-galactan side-chains, which contain carbohydrate  
81 decorations (**Fig. 1ab**). Glycans, comprising 90% of AGPs, are O-linked to hydroxyprolines  
82 in the protein component<sup>16</sup>. AGP utilisation is poorly understood. Oligosaccharide side-

83 chains are released by GH43 subfamily 24 (GH43\_24) exo-acting  $\beta$ 1,3-galactanases<sup>17</sup>,  
84 however, the mechanism for their unusual substrate specificity remains unclear. Although  
85 endo-acting enzymes contribute to glycan degradation, the role of endo-galactanases in  
86 AGP metabolism is unknown. While some enzymes that target AGPs have been  
87 described<sup>18,19</sup>, models for the degradation of these glycoproteins are lacking. The prebiotic  
88 potential of GA-AGPs is evident<sup>20</sup>, however, fulfilling the health benefit of these glycans  
89 requires a deeper understanding of how these proteoglycans are metabolised by the HGM.

90

91 Here we report a model for simple and complex AGP utilisation by *Bacteroides* species of  
92 the HGM. We reveal mechanisms of substrate specificity and catalysis of exo-acting  $\beta$ 1,3-  
93 galactanases. Strategies for removing the L-rhamnopyranose (Rhap) cap of complex AGPs  
94 were shown to influence synergetic interactions between side-chain degrading GHs and  
95 PLs. Critically, the cellular location of the endo- $\beta$ 1,3-galactanase defined whether a  
96 bacterium was a keystone organism, or a recipient of AGP-derived oligosaccharides.

97

## 98 **Results**

99

100 **Functional significance of  $PUL_{AGPS}$  and  $PUL_{AGPL}$  in *B. thetaiotaomicron*.** Previous data  
101 identified two PULs ( $PUL_{AGPL}$  and  $PUL_{AGPS}$ ) upregulated when *Bacteroides thetaiotaomicron*  
102 was cultured on larchwood AGP (LA-AGP) (**Fig. 1ac**)<sup>21</sup>. Here we showed that only  $PUL_{AGPS}$   
103 was substantially activated by GA-AGP (**Supplementary Fig. 1a**), suggesting that different  
104 molecules activate the two PULs. Growth studies of mutants of *B. thetaiotaomicron* lacking  
105 the two AGP PULs showed that  $\Delta PUL_{AGPL}$  failed to grow on LA-AGP but displayed growth on  
106 GA-AGP treated with endo- $\beta$ 1,3-galactanases (**Supplementary Fig. 2**).  $\Delta PUL_{AGPS}$  grew on  
107 LA-AGP but poorly on treated GA-AGP (**Supplementary Fig. 2**). These data suggest that  
108 the two PULs orchestrate the degradation of different AGPs. To explore the biochemical  
109 basis for these phenotypes, the specificity of the enzymes encoded by these loci were  
110 determined (**Supplementary Table 1**). Models for metabolism of selected AGPs were  
111 generated (**Fig. 1ab**).

112

113 **Cleavage of the galactan backbone.** Known activities within GH families the  $\beta$ -1,3-galactan  
114 backbone is depolymerized by GH43 subfamily 24 (GH43\_24)<sup>22</sup> and/or GH16<sup>23</sup> enzymes.  
115 Thus, activity of *B. thetaiotaomicron* GH43\_24 enzymes [BT0264, BT0265, BT3683 (also  
116 contains a GH16 module) and BT3685] encoded by  $PUL_{AGPL}$  and  $PUL_{AGPS}$  were evaluated  
117 against D-galactose (Gal) disaccharides, LA-AGP, GA-AGP, and linear  $\beta$ -1,3-galactan.  
118 Based on activity against disaccharides (**Supplementary Table 2**), and an active site pocket



119 (BT3683 and BT0265) in which O3 of bound Gal was not solvent exposed (**Fig. 3cd**),  
120 BT0265, BT3683 and BT3685 are exo-acting  $\beta$ -1,3-galactosidases. BT0265 and BT3683  
121 were active against LA-AGP and GA-AGP releasing oligosaccharide side-chains (**Fig.**  
122 **2abc**). Mutational analysis (**Supplementary Table 3**) showed that only the GH43\_24  
123 module contributed to the observed activity of BT3683. Consistent with other GH43\_24  $\beta$ -  
124 1,3-galactosidases<sup>17</sup>, the oligosaccharides generated by BT0265 and BT3683 likely  
125 comprise  $\beta$ -1,6-galactooligosaccharide side-chains. This assumption suggests that in  
126 BT0265 and BT3683, O6 of the Gal backbone units bound in the active site were solvent  
127 exposed enabling side-chain accommodation. BT3685 was more active against  $\beta$ -1,3-  
128 galactobiose than the other GH43\_24 enzymes, but was inactive against the AGPs tested.  
129 The role of the enzyme in degrading AGPs is unclear. The GH43\_24 enzyme BT0264 was  
130 inactive against galactobiose, released oligosaccharides from LA- and GA-AGP, and  
131 generated a range of oligosaccharides from  $\beta$ 1,3-galactan with the smaller products  
132 increasing with time (**Fig. 2d**); consistent with endo-activity.

133

134 ***Synergistic interactions in the degradation of the  $\beta$ -1,3-galactan backbone.*** In addition  
135 to O6-linked side chains, the AGP backbones contain sugar pendants at O2 or O4,  
136 commonly  $\beta$ -L-Araf units. These substitutions block progression of the exo- $\beta$ 1,3-  
137 galactanases through steric constraints (**Fig. 3**). Mechanisms for relieving these  
138 “roadblocks” include removal of these decorations and/or endo-cleavage of the backbone  
139 creating non-reducing termini downstream of O2/O4 decoration. To explore these  
140 hypotheses GA- and LA-AGP were incubated with BT3674, which contains an active-site  
141 typical of  $\beta$ -L-arabinofuranosidases (**Supplementary Fig. 3**). The enzyme released  
142 arabinose from LA-AGP, mediating an eight-fold increase in oligosaccharides generated by  
143 the exo- $\beta$ 1,3-galactanases (**Fig. 2a**). The endo- $\beta$ 1,3-galactanase BT0264 also increased the  
144 activity of the exo- $\beta$ 1,3-galactanases (**Fig. 2bc**). Thus, *B. thetaiotaomicron* exploits two  
145 mechanisms to reduce stalling of exo- $\beta$ 1,3-galactanases.

146

147 **Crystal structures of GH43\_24 enzymes.** The crystal structures of BT0265 and BT3683  
148 revealed that both exo- $\beta$ -1,3-galactosidases displayed a five-bladed  $\beta$ -propeller fold (**Fig. 3a**)  
149 typical of GH43 enzymes<sup>24</sup>. Typical of GH43 exo-glycosidases the active-site pocket of  
150 BT0265 and BT3683 is in the centre of the  $\beta$ -propeller<sup>24</sup>. Ligand complexes revealed the  
151 polar interactions between Gal, hexasaccharide product and Gal-based inhibitors and the  
152 exo- $\beta$ -1,3-galactosidases, **Fig. 3bcd**. These polar interactions are augmented by apolar  
153 contacts with a hydrophobic platform (Trp261/Trp213 in BT3683/BT0265). Interaction of the  
154 essential glutamate, Glu86/Glu87 in BT0265/BT3683 (**Supplementary Table 3**), with the

155 axial O4 of Gal (**Fig. 3bd**) confers selectivity for Gal over Glc, and is thus a key specificity  
156 determinant. O3 of bound ligands points into the active site pocket explaining the exo- and  
157 not endo-activity of the  $\beta$ 1,3-galactanases. The lack of interactions with substrate outside of  
158 the active site indicates that complementarity of the helical conformation of  $\beta$ 1,3-galactan<sup>25</sup>  
159 and topology of the catalytic centre drives specificity.

160

161 The BT0265 hexasaccharide product complex reveals O6 of Gal in the active site is solvent  
162 exposed (**Fig. 3b**). This explains why the enzyme releases backbone Gal residues  
163 decorated with oligosaccharides appended at O6. Whether side-chains contribute to  
164 specificity is unclear; however, elements of these decorations interact with BT0265 (**Fig. 3b**),

165

166 In GH43 enzymes the catalytic acid (glutamate) and  $pK_a$  modulator (aspartate) are  
167 invariant<sup>24</sup>. The assignment of Glu240 in BT3683 as the catalytic acid (**Fig. 3d**) is supported  
168 by the reactivity of E240A. This variant did not hydrolyse  $\beta$ 1,3-galactobiose but hydrolysed  
169 2,4-dinitrophenyl- $\beta$ -D-Gal (**Supplementary Table 3**), consistent with requiring protonation  
170 when Gal is the leaving group but not when 2,4-dinitrophenolate ( $pK_a$  3.6) is generated.  
171 Mutation of the catalytic acid in BT3685 (E225Q) also revealed the expected impact on  
172 activity against the two substrates. GH43\_24 enzymes lack the aspartate catalytic base that  
173 is invariant in other GH43 subfamilies<sup>24</sup>. In GH43\_24 a highly conserved glutamine binds a  
174 water molecule (**Fig. 3d**) that could attack the anomeric carbon of the substrate below the  
175 plane of the ring, consistent with the inverting mechanism of BT3685 (**Supplementary Fig.**  
176 **4**). Mutation of the glutamine in BT3683 supports a catalytic role for this residue  
177 (**Supplementary Table 3**). The glutamine may form an imidic acid through tautomerization  
178 and thus function as the base, as proposed for some inverting enzymes<sup>26</sup>, or assist in  
179 positioning the catalytic water that attacks the anomeric centre of the substrate.

180

181 **Deconstruction of the AGP side chains.** The side-chains, released by exo- $\beta$ 1,3-  
182 galactosidases from GA-AGP were characterized by mass spectrometry (**Supplementary**  
183 **Fig. 5**) and NMR spectroscopy (**Supplementary Fig. 6**). The major side chains comprised  
184 oligosaccharides with a degree of polymerization (DP) of 3 to 7 (**Supplementary Fig. 5**).  
185 The non-reducing terminus of each oligosaccharide comprised Rhap- $\alpha$ 1,4-GlcA- $\beta$ 1,6-Gal.  
186 Previous studies showed that the *B. thetaiotaomicron* GH145  $\alpha$ -L-rhamnosidase BT3686  
187 removed Rhap exposing GlcA<sup>19</sup>. Here we show that the exposed GlcA was removed by the  
188  $\beta$ -glucuronidase BT3677, the founding member of GH154 (**Fig. 4, Supplementary Fig. 7a,**  
189 **Supplementary Table 2**). BT3677 was only active against oligosaccharides after removal of  
190 the terminal Rhap, and is thus exo-acting. The  $\beta$ -glucuronidase hydrolysed the GlcA- $\beta$ 1,6-

191 Gal linkage when Gal was substituted with  $\alpha$ -L-Ara at O3 (**Fig. 4**) but not at O4  
192 (**Supplementary Fig. 8**).

193

194 *B. thetaiotaomicron* removes the terminal disaccharide structure of GA-AGP by a  
195 rhamnosidase-glucuronidase (RG) pathway, consistent with limited growth of  $\Delta bt3686$  on  
196 GA-AGP (**Supplementary Fig. 2b**). Cell-free extracts of  $\Delta bt3686$  cultured on LA-AGP failed  
197 to release Rhap from GA-AGP. These data confirm the RG pathway operates in *B.*  
198 *thetaiotaomicron* and that the side chains in GA-AGP are extensively capped with Rhap. The  
199 orthologues of BT3686 in *B. cellulosilyticus*, and other HGM *Bacteroidetes* species are not  
200 functional rhamnosidases as they lack the catalytic histidine<sup>19</sup>. *B. cellulosilyticus*, however,  
201 contains a rhamno-glucurono lyase (BACCELL\_00875) that cleaved the Rha- $\alpha$ 1,4-GlcA  
202 linkage, and the resultant 4,5 $\Delta$ GlcA was released by an unsaturated glucuronidase<sup>18</sup>. Thus,  
203 *B. cellulosilyticus* releases the capping Rha-GlcA disaccharide through a lyase-unsaturated  
204 glucuronidase (LU) pathway. Genomic studies indicate that both routes to removing the  
205 capping disaccharide (RG and/or LU pathways) are possible in some *Bacteroidetes* species.  
206 The significance of deploying both pathways is discussed below.

207

208 Gal at the base of AGP  $\beta$ -1,6-galactan side-chains can be decorated with Araf that may be  
209 capped with  $\alpha$ -Gal. No enzyme encoded by *B. thetaiotaomicron* AGP PULs removed the  $\alpha$ -  
210 Gal (discussed below). PUL<sub>AGPS</sub> also encodes two arabinofuranosidases; a GH43 enzyme  
211 (BT3675) and the non-specific arabinofuranosidase, BT3679, active against wheat AGP  
212 (WH-AGP), arabinoxylan and sugar beet arabinan (**Supplementary Fig. 7b**,  
213 **Supplementary Table 2**). BT3679 establishes a GH family (GH155) exclusive to the  
214 *Bacteroidetes* phylum. Cleavage of 4-nitrophenyl- $\alpha$ -L-arabinofuranoside by BT3679 in the  
215 presence of methanol generated methyl- $\alpha$ -arabinofuranoside (**Supplementary Fig. 7c**),  
216 demonstrating a retaining mechanism. In GA-AGP BT3679 cleaved the Araf- $\alpha$ 1,3-Gal  
217 linkage at the base of the  $\beta$ 1,6-galactan backbone irrespective of whether the Gal was  
218 decorated at O4 (**Supplementary Fig. 8**). BT3675 hydrolysed the Araf- $\alpha$ 1,3-Gal glycosidic  
219 bond, but not when Gal also contained  $\alpha$ -L-Araf at O4. The two enzymes and cell-free  
220 extracts of *B. thetaiotaomicron* cultured on AGPs did not cleave the O4-linked Araf. Thus, *B.*  
221 *thetaiotaomicron* is unable to cleave  $\alpha$ -Araf linked O4 to Gal.

222

223 The GH35 enzyme BT0290 hydrolysed  $\beta$ -1,6-galactan side-chains in LA-AGP and  $\beta$ -1,6-  
224 galactobiose, exhibiting minor activity against  $\beta$ -1,3-galactobiose. The crystal structure of  
225 BT0290 revealed a ( $\beta/\alpha$ )<sub>8</sub> barrel catalytic module. In the ligand complex Gal is in the active

226 site pocket at the end of the  $\beta$ -barrel (**Supplementary Fig. 9**), which contains a pair of  
227 glutamates that comprise a canonical catalytic apparatus for a retaining enzyme, expected  
228 for GH35. The pocket extends onto a planar surface that houses the O6-linked  $\beta$ -Gal in the  
229 +1 subsite. Trp215 in the +1 subsite creates a steric block for O3- or O4-linked sugars and  
230 provides a hydrophobic platform for an O6-linked  $\beta$ -Gal. This tryptophan is likely a specificity  
231 determinant for the  $\beta$ -1,6-galactosidase activity of BT0290.

232

233 ***In vivo* degradation of AGPs by HGM Bacteroidetes species. Supplementary Table 4**  
234 reports growth profiles of type strains of 20 HGM *Bacteroidetes* species. All species except  
235 *Dysgonomonas gadei* utilised LA-AGP, while only *B. cellulosilyticus*, *B. caccae* and *D. gadei*  
236 grew on GA-AGP or WH-AGP (**Supplementary Table 4**). This was surprising as *B.*  
237 *thetaitaomicron*, at least, degrades side-chains from GA-AGP. The initial depolymerisation  
238 of polysaccharides in *Bacteroides* species occurs at the bacterial surface, generating  
239 oligosaccharides suitable for transport into the periplasm<sup>10,11</sup>. In *B. thetaitaomicron* the  
240 GH43\_24 endo- $\beta$ 1,3-galactanase, BT0264, has a type I signal peptide typical of periplasmic  
241 proteins, confirmed by cell localization studies (**Fig. 5a, Supplementary Fig. 10**). The  
242 inability of *B. thetaitaomicron* to grow on GA-AGP likely reflects the absence of a surface  
243 endo- $\beta$ 1,3-galactanase required to generate the GA-AGP-derived oligosaccharides for  
244 import into the periplasm. This was confirmed by growth of *B. thetaitaomicron* on GA-AGP  
245 and WH-AGP pre-treated with BT0264 (**Fig. 5bc, Supplementary Table 4**). The BT0264-  
246 treated GA-AGP was also a growth substrate for the other 16 *Bacteroidetes* species unable  
247 to utilise intact GA- and WH-AGP (**Supplementary Table 4**). The inability of the majority of  
248 HGM-derived *Bacteroidetes* species to utilise GA-AGP reflects the lack of an endo- $\beta$ 1,3-  
249 galactanase that can degrade extracellular GA-AGP. Growth of these organisms on LA-AGP  
250 reflects the low DP of the glycan, enabling direct import into the periplasm.

251

252 The *B. cellulosilyticus* genome encodes four GH16 and four GH43\_24 enzymes that,  
253 potentially, comprise endo- $\beta$ 1,3-galactanases. RT-PCR of SusC genes of three PULs  
254 encoding enzymes from these families (**Supplementary Fig. 1b**), revealed only one locus  
255 (contains three *susCs*) that was significantly upregulated by AGPs (**Supplementary Fig.**  
256 **1c**). Of the GH43\_24 and GH16 enzymes encoded by these PULs, only Baccell00844  
257 (GH16) degraded  $\beta$ 1,3-galactan and is thus an endo- $\beta$ 1,3-galactanase (**Fig. 5d**). Baccell-  
258 00844 contains a type II signal peptide, consistent with a surface location. Whole cell assays  
259 of *B. cellulosilyticus* under aerobic conditions, which report only activity of surface proteins<sup>11</sup>,  
260 showed that  $\beta$ 1,3-galactan was degraded into numerous oligosaccharides (**Fig 5e**). This  
261 indicates that *B. cellulosilyticus* displays surface endo- $\beta$ 1,3-galactanase activity, which is

262 likely mediated by Baccell00844. Support for the role played by Baccell00844 is provided by  
263 growth of all the *Bacteroidetes* species on GA-AGP pre-treated with Baccell00844  
264 (**Supplementary Table 4**). An orthologue to Baccell00844 in *B. caccae* (BACCAC\_03237)  
265 may explain its growth on GA-AGP and WH-AGP. Insertion of *bacell00844* into *B.*  
266 *thetaitaomicron* PUL<sub>AGPL</sub> (*B. thetaitaomicron::bacell00844*) enabled the bacterium to  
267 grow on intact GA-AGP and WH-AGP (**Fig. 5bc**). *B. thetaitaomicron::bacell00844*, but not  
268 wild type *B. thetaitaomicron*, degraded  $\beta$ 1,3-galactan in aerobic whole cell assays (**Fig. 5e**)  
269 demonstrating acquisition of surface endo- $\beta$ 1,3-galactanase activity. Proteomic analysis of  
270 intact cells of *B. thetaitaomicron::bacell00844* revealed tryptic peptides from 46 proteins  
271 (**Fig 5f**) that were detected only on the bacterial surface. These proteins included Baccell-  
272 00844 (five tryptic peptides identified by MS/MS, **Supplementary Fig. 11**). Among the 45 *B.*  
273 *thetaitaomicron* proteins were a number that have been shown, experimentally, to be  
274 surface exposed (SusD/C-like proteins, surface CAZymes and SGBPs; **Supplementary**  
275 **Table 5**), and all the polypeptides contain canonical type II signal peptides consistent with  
276 outer membrane attachment. The presence of Baccell00844 among these 46 proteins  
277 supports its proposed surface location in *B. thetaitaomicron::bacell00844*. Collectively, the  
278 proteomics data and surface endo- $\beta$ 1,3-galactanase activity of *B.*  
279 *thetaitaomicron::bacell00844* demonstrates that growth of the engineered bacterium on  
280 intact GA-AGP and WH-AGP is conferred through the surface endo- $\beta$ 1,3-galactanase  
281 activity encoded by *bacell00844*.

282

283 Data presented above suggest *B. thetaitaomicron::bacell\_00844*, in addition to *B.*  
284 *cellulosilyticus*, *B. caccae* and *D. gadei* are keystone organisms for AGP utilisation by  
285 Bacteroidetes. To test this hypothesis two of the organisms that cannot grow on untreated  
286 GA-AGP, wild type *B. thetaitaomicron* and *B. ovatus*, were co-cultured with *B.*  
287 *thetaitaomicron::bacell\_00844*, *B. cellulosilyticus* and *B. caccae* on the intact glycan, and  
288 the bacteria in the co-cultures were quantified by quantitative-PCR of genomic-specific  
289 sequences. CFUs of wild type *B. thetaitaomicron* and *B. ovatus* increased (**Fig. 6**) and thus  
290 these organisms grew on GA-AGP in the presence, but not in the absence, of *B.*  
291 *cellulosilyticus*, *B. caccae* or *B. thetaitaomicron::bacell\_00844*. This indicates that *B.*  
292 *cellulosilyticus*, *B. thetaitaomicron::bacell\_00844* or *B. caccae* provide GA-AGP-derived  
293 oligosaccharides as growth substrates for the recipient bacteria. These data establish *B.*  
294 *cellulosilyticus*, *B. thetaitaomicron::bacell\_00844* and *B. caccae*, and by inference *D.*  
295 *gadei*, as keystone bacteria in the utilisation of complex AGPs, with *B. thetaitaomicron*, *B.*  
296 *ovatus*, and likely other Bacteroidetes, comprising recipient organisms. *B. thetaitaomicron*  
297 and *B. ovatus* demonstrate a preference for products released by *B. cellulosilyticus* and *B.*

298 *caccae*, respectively, providing possible examples of discrete AGP cross-feeding niches  
299 provided by each keystone organism.

300

301 To establish the extent to which *B. thetaiotaomicron* utilizes AGP side-chains, limit products  
302 generated from growth on BT0264-treated GA-AGP were characterized. The major product  
303 was a hexasaccharide derived from a heptasaccharide in which the terminal rhamnose had  
304 been removed by BT3686 (**Supplementary Fig. 12 and 13**). The inability to degrade this  
305 oligosaccharide reflects the absence of a  $\alpha$ -galactosidase encoded by the AGP-PULs,  
306 preventing BT3679 from accessing the 3-linked *Araf*. The limit product generated by *B.*  
307 *cellulosilyticus* from GA-AGP was a tetrasaccharide, also derived from the heptasaccharide  
308 (**Supplementary Fig. 12 and 13**). This is consistent with the  $\alpha$ -galactosidase gene  
309 *bacell00859* in the *B. cellulosilyticus* AGP PUL, and removal of the Rha-GlcA cap by the LU  
310 pathway in which the unsaturated glucuronidase can target 4,5 $\Delta$ GlcA- $\beta$ 1,6-Gal linkages in  
311 which the Gal is decorated at O3 and/or O4. Both organisms lacked an  $\alpha$ -  
312 arabinofuranosidase that targeted O4 linkages.

313

314 **Analysis of AGP-PULs in HGM Bacteroidetes species.** Only *B. finegoldii* contained a  
315 locus equivalent to *B. thetaiotaomicron* PUL<sub>AGPL</sub>, while PUL<sub>AGPs</sub> was in most species of the  
316 *Bacteroides* genus, with various levels of rearrangements (**Supplementary Fig. 14 and 15**).  
317 No enzyme conservation pattern that correlated with growth on LA-AGP or GA-AGP was  
318 identified. For example, *B. stercoris* grows on LA-AGP but lacks the orthologous enzymes  
319 found in its closest relatives. The evolution of AGP-PULs was compared to the (16S-based)  
320 phylogenetic tree of the species (**Supplementary Table 4**). Closely-related species have  
321 similar PUL organization, but at the single gene level there are examples of a lack of  
322 orthologues. Thus Bacteroidetes AGP PULs are highly dynamic systems that can be rapidly  
323 lost, gained, or rearranged between closely related species (see *B. massiliensis* and *B.*  
324 *plebeius* in comparison with *B. vulgatus* and *B. dorei*; *B. cellulosilyticus* compared to *B.*  
325 *thetaiotaomicron*). In consequence 16S-derived taxonomy cannot be used to predict AGP  
326 degradation in Bacteroidetes.

327

## 328 **Discussion**

329 This study reveals the enzymes required to depolymerise the  $\beta$ 1,3-galactan backbone of  
330 AGPs, resulting in release of the oligosaccharide side-chains. This diversity likely reflects the  
331 substituents at O2 or O4 of the backbone Gals that would limit the progressive action of the  
332 critical exo-galactanases. The data also show that the GH43 exo- $\beta$ 1,3-galactanases lack the

333 catalytic base present in all other enzymes of this family. Deviation from conservation of  
334 catalytic residues in GH families is rare, although not without precedent<sup>27</sup>.

335

336 Analysis of the enzymes that deconstruct side-chains of two AGPs provides insights into the  
337 biological relevance of the AGP PULs in *B. thetaiotaomicron*. The inability of  $\Delta$ PUL<sub>AGPL</sub> to  
338 grow on LA-AGP reflects the absence of BT0290, the  $\beta$ 1,6-galactosidase that hydrolyses the  
339  $\beta$ 1,6-galactan side-chains which, in this glycan, are not extensively decorated. BT0290 is  
340 less important in degrading complex AGPs, such as GA-AGP, as the decoration of  $\beta$ 1,6-  
341 galactan side-chains with other sugars represent significant nutrients. The inability of  
342  $\Delta$ PUL<sub>AGPS</sub> to grow on GA-AGP (endo- $\beta$ 1,3-galactanase pre-treated) reflects extensive  
343 capping of the side chains with Rhap. Loss of the rhamnosidase gene *bt3686* in PUL<sub>AGPS</sub>  
344 greatly restricts further degradation of the side-chains. To summarise, PUL<sub>AGPS</sub> encodes an  
345 enzyme consortium that degrades the major side chains in complex AGPs such as GA-AGP,  
346 while PUL<sub>AGPL</sub> targets the  $\beta$ -1,6,linked Gal side chains that are important nutrients in simpler  
347 glycans such as LA-AGP.

348

349 AGPs are diverse and numerous enzymes are required to mediate their deconstruction.  
350 Combined with recent reports<sup>18,19</sup>, four CAZyme families that contribute to AGP degradation  
351 were discovered, however, further enzymes likely await discovery. Indeed, in PUL<sub>AGPL</sub> there  
352 are 14 genes encoding secreted hypothetical proteins that may contribute to degradation of  
353 complex AGPs not investigated here. Unusually, two different pathways remove the  
354 disaccharide that caps the side-chains in GA-AGP. Although the more flexible LU pathway  
355 should enable more comprehensive degradation, several HGM *Bacteroides* species utilise  
356 the RG pathway that limits downstream processing of the oligosaccharides. The contrasting  
357 oligosaccharide utilisation profiles observed between *B. thetaiotaomicron* and *B.*  
358 *cellulosilyticus* (**Supplementary Fig. 11**), and predicted by differences in the AGP PULs in  
359 other *Bacteroides* spp. (**Supplementary Fig. 12 and 13**), may enable co-existence of  
360 species within a common niche targeting different components of the same glycan.

361

362 The majority of *Bacteroidetes* species studied here were unable to utilise GA-AGP, although  
363 they grow on the glycan after backbone cleavage. Utilisation of complex AGP by the HGM  
364 *Bacteroidetes* relies on the extracellular endo-activity of a few keystone species. This study  
365 in conjunction with recent reports<sup>28,29</sup> shows that glycan cross-feeding between HGM  
366 *Bacteroides* species contributes to the ecology of carbohydrate utilisation in this ecosystem.  
367 Nevertheless *Bacteroides* glycan degrading systems generally contain surface endo-acting

368 enzymes that generate fragments which are imported into the periplasm<sup>10,11</sup>, obviating the  
369 requirement for cross-feeding to utilise the polysaccharide.

370

371 In conclusion, dissecting mechanisms by which AGPs are degraded by HGM *Bacteroidetes*  
372 species reveals enzyme families of potential biotechnological relevance, and shows how  
373 synthetic biology can be used to engineer organisms to degrade AGPs that are abundant in  
374 the human diet.

375

376

## 377 **METHODS**

378

### 379 **Cloning, expression and purification of recombinant proteins**

380 DNAs encoding enzymes lacking their signal peptides were amplified by PCR using  
381 appropriate primers. The amplified DNAs were cloned into pET28a with an N-terminal His<sub>6</sub>  
382 tag using NheI and XhoI restriction sites (Table 3SM). The genes were then expressed in *E.*  
383 *coli* BL21, or Tuner cells, transformed with the appropriate recombinant plasmids. The  
384 transformed *E. coli* strains were cultured in Luria broth (LB) supplemented with 10 µg/ml of  
385 kanamycin. Cultured cells were grown at 37 °C to mid-log phase and induced with 1 mM  
386 isopropyl β-D-1-thiogalactopyranoside at 16 °C overnight. Cells were pelleted by  
387 centrifugation at 5,000 rpm for 10 min and resuspended in 20 mM Tris-HCl buffer, pH 8.0,  
388 containing 300 mM NaCl. For selenomethionine-derivatized protein the above procedure  
389 was used but adjusted as follows: *E. coli* B834 cells were transformed with the appropriate  
390 recombinant plasmid. Overnight 5-ml cultures, in LB, were then used to inoculate 100 ml of  
391 LB culture in a 250-ml flask, which was then grown to an O.D. of 0.4. A methionine-deficient  
392 media was prepared using the Molecular Dimensions SelenoMet™ Medium Base (MD12-  
393 501) and SelenoMet™ Nutrient mixtures (MD12-502) and was used to wash the cultured  
394 B834 cells. The cells were then inoculated into 1 liter of methionine-deficient media to which  
395 selenomethionine was added to a final concentration of 5 mg/ml. Cells were collected and  
396 disrupted by sonication, and the cell-free extract was recovered by centrifugation at 15,000  
397 rpm for 30 min. Recombinant proteins were purified from the cell-free extract using  
398 immobilized metal affinity chromatography using Talon™, a cobalt-based matrix. Proteins  
399 were eluted from the column in Buffer A containing 100 mM imidazole. For crystallographic  
400 studies, BT0265, BT0290, BT3674, BT3679, and BT3683 were further purified by size  
401 exclusion chromatography using a Superdex S200 16/600 column equilibrated with Buffer A  
402 on a fast protein liquid chromatography system (ÅKTA FPLC; GE Healthcare). All proteins  
403 were purified to electrophoretic homogeneity as judged by SDS-PAGE.

404

### 405 **Mutagenesis**

406 Site-directed mutagenesis was conducted using the PCR-based QuickChange site-directed  
407 mutagenesis kit (Stratagene) according to the manufacturer's instructions, using the  
408 appropriate plasmid encoding BT0290, BT3674, BT3683 and BT3685 as the template and  
409 appropriate primer pairs.

410

411

### 412 **Large scale purification of oligosaccharides**

413 GA-AGP derived oligosaccharides were generated by incubating 20 g of the glycan with 1  
414 µM of the β1,3-galactosidase BT0265 in 20 mM sodium phosphate buffer pH 7.0  
415 implemented with 150 mM NaCl at 37 °C for 16 h. The oligosaccharide mixture was freeze  
416 dried and resuspended in water before being applied to a P2-BioGel (BioRad) column with a  
417 0.22 ml/min flow rate. Fractions were evaluated for oligosaccharide content and purity by



418 TLC. Pure fractions of defined oligosaccharides were pooled and concentrated.  
419 Oligosaccharide size was confirmed by Mass Spectrometry and HPAEC.

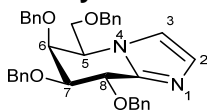
420

### 421 Chemical synthesis

422 The synthesis of 2,4-dinitrophenyl- $\beta$ -D-galactopyranoside was as described previously<sup>31</sup>

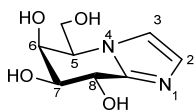
423

### 424 (5*R*,6*S*,7*S*,8*R*)-5-[(Benzyloxy)methyl]-6,7,8-tri(benzyloxy)-5,6,7,8- 425 tetrahydroimidazo[1,2-*a*]pyridine



426 5-Amino-2,3,4,6-tetra-O-benzyl-5-deoxy-1-thio-D-galactono-1,5-lactam<sup>32</sup>  
427 (61.5 mg, 0.111 mmol) was dissolved in aminoacetaldehyde dimethyl acetal (0.18 mL, 1.652  
428 mmol) and stirred under N<sub>2</sub> for 24 h. The mixture was diluted with EtOAc (20 mL) and  
429 washed with H<sub>2</sub>O (2 × 20 mL) and brine (1 × 20 mL). The organic extracts were dried  
430 (MgSO<sub>4</sub>) and then concentrated under reduced pressure. The crude residue was dissolved  
431 in toluene (3.2 mL) and H<sub>2</sub>O (0.3 mL). *p*-Toluenesulfonic acid monohydrate (54.9 mg, 0.289  
432 mmol) was added to the solution and the reaction mixture was stirred at 65 °C for 18 h. The  
433 mixture was diluted with EtOAc (20 mL) and washed with NaHCO<sub>3</sub> (2 × 20 mL) and brine (1  
434 × 20 mL). The organic extracts were dried (MgSO<sub>4</sub>), concentrated and the resulting residue  
435 was subjected to flash chromatography (EtOAc/pet. spirits 8:2) to afford the protected  
436 galactonoimidazole (49.1 mg, 79% over two steps) as a colourless oil; [α]<sub>D</sub><sup>26</sup> +73 (c 1.36,  
437 CHCl<sub>3</sub>); <sup>1</sup>H NMR (500 MHz, CDCl<sub>3</sub>): δ 3.74 (1 H, dd, *J*<sub>5,6</sub> = 10.2, *J*<sub>6,7</sub> = 8.3 Hz, H6), 4.02 (2 H,  
438 m, H8, H7), 4.34 (1 H, dd, *J*<sub>5,5'</sub> = 1.9, *J*<sub>5',5</sub> = 5.8 Hz, CH<sub>2</sub>(C5)), 4.44 (3 H, m, CH<sub>2</sub>(C5), H5,  
439 CH<sub>2</sub>Ph), 4.55 (2 H, m, 2 × CH<sub>2</sub>Ph), 4.62 (2 H, m, 2 × CH<sub>2</sub>Ph), 4.71 (2 H, m, 2 × CH<sub>2</sub>Ph), 4.90  
440 (1 H, d, *J* = 11.9 Hz, CH<sub>2</sub>Ph), 7.03 (1 H, d, *J*<sub>2,3</sub> = 1.3 Hz, H3), 7.14 (1H, d, *J*<sub>2,3</sub> = 1.3 Hz, H2),  
441 7.18-7.32 (20 H, m, 4 × Ph); <sup>13</sup>C NMR (125 MHz, CDCl<sub>3</sub>): δ 57.5 (1 C, C5), 71.5 (1 C,  
442 CH<sub>2</sub>Ph), 71.7 (1 C, C7), 72.0 (1 C, C6), 71.4 (1 C, CH<sub>2</sub>Ph), 72.9 (1 C, CH<sub>2</sub>Ph), 73.5 (1 C,  
443 CH<sub>2</sub>Ph), 73.7 (1 C, C5'), 77.6 (1 C, C8), 119.5 (1 C, C2), 129.2 (1 C, C3), 127.7-138.4 (20 C,  
444 4 × Ph), 142.1 (C8') ppm; HRMS (ESI)<sup>+</sup> *m/z* 561.2751 [C<sub>36</sub>H<sub>36</sub>N<sub>2</sub>O<sub>4</sub> (M+H)<sup>+</sup> requires  
445 561.2748].

### 446 (5*R*,6*S*,7*S*,8*R*)-5-[(Hydroxymethyl)-6,7,8-triol-5,6,7,8-tetrahydroimidazo[1,2-*a*]pyridine 447 (Galacto-imidazole; Gal-Im)



448 Pd(OH)<sub>2</sub>/C (20%, 46.2 mg) was added to a solution of EtOAc/MeOH/H<sub>2</sub>O  
449 (5:17:3, 1.0 mL), AcOH (0.44 mL) and the protected imidazole (24.6 mg, 0.044 mmol). The  
450 reaction vessel was filled with H<sub>2</sub> (34 bar) and agitated for 41 h. The suspension was filtered  
451 through a Celite pad and subjected to flash chromatography (EtOAc/MeOH/H<sub>2</sub>O 8:2:1) to  
452 afford the target (8.5 mg, 96%) as an amorphous solid; m.p. 82 °C; [α]<sub>D</sub><sup>23</sup> +22 (c 0.435,  
453 MeOH); <sup>1</sup>H NMR (500 MHz, CD<sub>3</sub>OD): δ 3.88 (1 H, dd, *J*<sub>6,7</sub> = 2.2, *J*<sub>7,8</sub> = 7.7 Hz, H7), 4.05 (2 H,  
454 apt. d, CH<sub>2</sub>(C5)), 4.28 (1 H, m, H5), 4.38 (1 H, dd, *J*<sub>5,6</sub> = 3.4, *J*<sub>6,7</sub> = 2.2 Hz, H6), 4.82 (1 H, d,  
455 *J*<sub>2,3</sub> = 7.7 Hz, H8), 7.19 (1 H, d, *J* = 1.1 Hz, H3), 7.51 (1H, d, *J* = 1.2 Hz, H2); <sup>13</sup>C NMR (125  
456 MHz, CD<sub>3</sub>OD): δ 61.6 (1 C, C5), 63.1 (1 C, C5'), 67.7 (1 C, C8), 70.5 (1 C, C6), 75.0 (1 C,  
457 C7), 119.9 (1 C, C2), 126.4 (1 C, C3), 147.6 (C8') ppm.

### 458 CAZyme Assays

459 Spectrophotometric quantitative assays for  $\beta$ -D-galactosidase BT0264, BT0290, BT3683 and  
460 BT3685;  $\beta$ -L-arabinofuranosidase BT3674;  $\alpha$ -L-arabinofuranosidases BT3675 and BT3679  
461 and the  $\beta$ -D-glucuronidase BT3677 were monitored by the formation of NADH, at A<sub>340 nm</sub>  
462 using an extinction coefficient of 6,230 M<sup>-1</sup> cm<sup>-1</sup>, with an appropriately linked enzyme assay

463 system. The assays were adapted from two Megazyme International assay kits; the L-  
464 arabinose/D-galactose assay kit (K-ARGA) and the  $\alpha$ -glucuronidase assay kit (K-AGLUA).  
465 Activity on 4-nitrophenyl-glycosides was monitored at  $A_{400\text{nm}}$ . The mode of action of enzymes  
466 were determined using high performance anion exchange chromatography (HPAEC) or TLC,  
467 as appropriate. In brief, aliquots of the enzyme reactions were removed at regular intervals  
468 and, after boiling for 10 min to inactivate the enzyme and centrifugation at 13,000g, the  
469 amount of substrate remaining or product produced was quantified by HPAEC using  
470 standard methodology. The reaction substrates and products were bound to a Dionex  
471 CarboPac PA100 (galactooligosaccharides/arabinooligosaccharides), PA1  
472 (monosaccharides) or PA20 (polygalacturonic acid oligosaccharides) column and glycans  
473 eluted with an initial isocratic flow of 100 mM NaOH then a 0–200 mM sodium acetate  
474 gradient in 100 mM NaOH at a flow rate of 1.0 ml min<sup>-1</sup>, using pulsed amperometric  
475 detection. Linked assays were checked to make sure that the relevant enzyme being  
476 analysed was rate limiting by increasing its concentration and ensuring a corresponding  
477 increase in rate was observed. A single substrate concentration was used to calculate  
478 catalytic efficiency ( $k_{\text{cat}}/K_M$ ), and was checked to be markedly less than  $K_M$  by halving and  
479 doubling the substrate concentration and observing an appropriate increase or decrease in  
480 rate. The equation  $V = (k_{\text{cat}}/K_M)[S][E]$  where  $V$  is the initial rate,  $[S]$  and  $[E]$  are substrate and  
481 enzyme concentration, respectively. All reactions were carried out in 20 mM sodium  
482 phosphate buffer, pH 7.0, with 150 mM NaCl (defined as standard conditions) and performed  
483 in at least technical triplicates.

484

#### 485 **Electrospray ionisation mass spectrometry (ESI-MS)**

486 The molecular mass of purified oligosaccharides (in 10 mM ammonium acetate, pH 7.0)  
487 were analysed via negative ion mode infusion/offline ESI-MS following dilution (typically 1:1  
488 (v/v)) with 5% trimethylamine in acetonitrile. Electrospray MS data was acquired using an  
489 LTQ-FT mass spectrometer (Thermo) with a FT-MS resolution setting of 100,000 at  
490  $m/z = 400$  and an injection target value of 1,000,000. Infusion spray analyses were  
491 performed on 5–10  $\mu\text{L}$  of samples using medium 'nanoES' spray capillaries (Thermo) for  
492 offline nanospray mass spectrometry in negative ion mode at 1 kV.

493

#### 494 **Liquid chromatography-mass spectrometry**

495 The sample containing the oligosaccharides generated by treatment of LA-AGP with BT0265  
496 was diluted 1:10 (v/v) with Buffer B (85% acetonitrile/15% 50 mM ammonium formate in  
497 water, pH 4.7) and 0.5  $\mu\text{L}$  was analysed by LC-MS analysis via elution from a ZIC-HILIC  
498 (SeQuant®, 3.5  $\mu\text{m}$ , 200 $\text{\AA}$ , 150 X 0.3 mm, Merck, UK) capillary column. The column was  
499 connected to a NanoAcquity HPLC system (Waters, UK) and heated to 35°C with an elution  
500 gradient as follows; 100% Buffer B for 5 min, followed by a gradient to 25% Buffer B/75%  
501 Buffer A (50 mM ammonium formate in water, pH 4.7) over 40 min. The flow rate was 5  
502  $\mu\text{L}/\text{min}$  and 10 column volumes of Buffer B equilibration was performed between injections.  
503 MS data was collected using a Bruker Impact II QToF mass spectrometer operated in  
504 positive ion mode, 50 – 2000  $m/z$ , with capillary voltage and temperature settings of 2800 V  
505 and 200 °C respectively, together with a drying gas flow and nebulizer pressure of 6 L/min  
506 and 0.4 Bar. The MS data was analysed using Compass DataAnalysis software (Bruker).

507

#### 508 **<sup>1</sup>H-NMR determination of catalytic mechanism**

509 The enzymes BT3685 and BT3679 at ~20  $\mu\text{M}$  were assayed using 2,4-dinitrophenyl- $\beta$ -D-  
510 galactopyranoside (5 mM) and 4-nitrophenyl  $\alpha$ -L-arabinofuranoside, respectively. The  
511 enzymes were solvent-exchanged three times by ultrafiltration in 20 mM Tris-HCl, 500 mM  
512 NaCl, pH 7.5 using D<sub>2</sub>O as the solvent. Substrates were repeatedly freeze dried using the  
513 same buffer and resuspended in D<sub>2</sub>O. Prior to addition of enzyme an initial <sup>1</sup>H-NMR  
514 spectrum was obtained. Enzyme was added and spectra were recorded at appropriate time  
515 intervals. The emergence of individual monosaccharide product  $\alpha$ - and  $\beta$ -anomers in the

516 case of BT3685 was monitored to deduce catalytic mechanism. The reaction catalyzed by  
517 BT3679 was carried out in the presence of 2.5 M methanol. The products were freeze-dried  
518 and resuspended in D<sub>2</sub>O. Spectra recorded were analysed for the chemical shift of the  
519 anomeric <sup>1</sup>H of the methyl L-arabinofuranoside product to determine mechanism.

520

## 521 **2D NMR and mass spectrometry of GA-AGP oligosaccharides**

522 **<sup>1</sup>H-NMR:** NMR spectra were recorded at 298 K in D<sub>2</sub>O with a Bruker AVANCE III  
523 spectrometer operating at 600 MHz equipped with a TCI CryoProbe. NMR chemical-shift  
524 assignments were obtained using 2D <sup>1</sup>H-<sup>1</sup>H TOCSY, ROESY and DQFCOSY alongside 2D  
525 <sup>13</sup>C HSQC, H2BC, HMBC, HSQC-TOCSY and HSQC-ROESY experiments using  
526 established methods<sup>33</sup>. The mixing times were 70 ms and 200 ms for the TOCSY and  
527 ROESY experiments, respectively (data for the tetra- and heptasaccharides are shown in  
528 **Supplementary Fig. 4**). Chemical shifts were measured relative to internal acetone ( $\delta_{\text{H}}$   
529 =2.225,  $\delta_{\text{C}}$ =31.07 ppm). Data were processed using the Azara suite of programs (v. 2.8,  
530 copyright 1993-2017, Wayne Boucher and Department of Biochemistry, University of  
531 Cambridge, unpublished) and chemical-shift assignment was performed using Analysis  
532 v2.4<sup>34</sup>. The non-reducing-end Rha residue was readily identified from the presence of a  
533 methyl group at the 6-position. All the linkages were clear from downfield <sup>13</sup>C shifts of the  
534 linked atoms, inter-glycosidic crosspeaks in the HMBC spectrum and intense NOE  
535 crosspeaks in the ROESY spectrum. The anomeric configurations of the pyranoses were  
536 confirmed by measurement of the <sup>1</sup>J<sub>C-1,H-1</sub> coupling constant (c. 170 and 160 Hz for  $\alpha$ - and  $\beta$ -  
537 configurations, respectively<sup>35</sup>) in an F1-coupled <sup>13</sup>C HSQC. The assignments were complete  
538 and are shown in **Supplementary Table 7**.

539

540 **Mass spectroscopy:** To confirm the AGP oligosaccharide chain structure suggested by  
541 NMR, the sample was per-methylated and analysed by MALDI ToF-MS and MS/MS. A  
542 single high intensity peak, with  $m/z$  1393.5 was identified which is consistent with the  
543 composition Ara<sub>2</sub>RhaGal<sub>3</sub>GlcA. The tandem mass spectrometry (MS/MS) spectrum of this  
544 per-methylated oligosaccharide is shown in **Supplementary Fig. 5**. The presence of Y<sub>1</sub> ( $m/z$   
545 259.0) and <sup>1,5</sup>X<sub>1</sub> ( $m/z$  287.0) indicates the reducing end is Gal. The <sup>0,4</sup>A<sub>4</sub> ( $m/z$  1217.5) cross-  
546 ring fragment indicates the presence of 1,6-linkage onto the reducing end Gal. Y<sub>3</sub> ( $m/z$   
547 1205.5) and <sup>1,5</sup>X<sub>3</sub> ( $m/z$  1233.4) indicate terminal Rha, Y<sub>3 $\alpha$</sub>  ( $m/z$  1175.4) and <sup>1,5</sup>X<sub>3 $\alpha$</sub>  ( $m/z$   
548 1203.4) indicate terminal Gal, and Y<sub>2 $\beta$</sub>  ( $m/z$  1219.5) and <sup>1,4</sup>X<sub>2  $\beta$</sub>  ( $m/z$  1247.5) terminal Ara  
549 residues. Y<sub>2</sub> ( $m/z$  987.3) indicates a terminal disaccharide Rha-GlcA. The 1,4-linkage  
550 between the terminal Rha and GlcA was confirmed by the cross ring fragments (<sup>3,5</sup>A<sub>2</sub> ion,  
551  $m/z$  313.0; <sup>0,2</sup>X<sub>2</sub> ion,  $m/z$  1043.3) and elimination ions (G<sub>3</sub> ion,  $m/z$  1157.4; E<sub>2</sub> ion,  $m/z$   
552 399.0). The non-reducing end <sup>0,4</sup>A<sub>3</sub> cross-ring fragment ( $m/z$  489.0) and H<sub>2</sub> elimination ion  
553 ( $m/z$  765.1) suggest the presence of 1,6-linkage between the GlcA and Gal. The 728 Da  
554 mass difference between the Y<sub>2</sub> and Y<sub>1</sub> ions suggests that there are two Gal and two Ara  
555 residues between the GlcA and the reducing end Gal. The G<sub>2</sub> ( $m/z$  807.1) indicates there is  
556 a single backbone residue of Gal. The presence of Y<sub>2 $\alpha$</sub>  ion ( $m/z$  987.3), but absence of an ion  
557 corresponding to loss of a dipentose side chain, indicates that the one of the side chains is a  
558 disaccharide of Gal linked to Ara. As described above, there is terminal Gal, so this structure  
559 is Gal-Ara. Substitution of O3 and O4 but not O2 of the Gal is suggested by the presence of  
560 G<sub>2</sub> ( $m/z$  807.1) and <sup>0,2</sup>X<sub>1</sub> ( $m/z$  315.0), ions. The H<sub>2</sub> elimination ion, which reflects loss of  
561 Rha-GlcA and Ara, suggests an Ara is linked to O4 of the Gal, which is supported by the  
562 presence of the <sup>3,5</sup>A<sub>3</sub> ( $m/z$  677.1). The elimination ions (G<sub>2</sub>,  $m/z$  807.1; D<sub>3</sub>,  $m/z$  779.1) suggest  
563 that the Gal-Ara disaccharide is linked to the O3 of the Gal on the backbone. The cross-ring  
564 fragment <sup>0,2</sup>X<sub>2 $\alpha$</sub>  ( $m/z$  1071.3) and elimination ion G<sub>3 $\alpha$</sub>  ( $m/z$  1113.3) suggests that the terminal  
565 Gal is not 1,2-linked to the Ara, but we were unable to locate further from the MS/MS the Gal

566 linkage, but the results are consistent with 1,3 linkage to the Ara. The presence of this G<sub>3α</sub>  
567 ion also indicates the furanose form of the Ara.

#### 568 **Growth of *Bacteroides* and generation of mutants**

569 *Bacteroides* mutants were generated by deletion of the target gene by counter selectable  
570 allelic exchange using the pExchange-tdk plasmid. The full method is described in Ref<sup>36</sup>.  
571 Mutants generated in this study are distinguished by the locus tag of the gene  
572 deleted/inactivated (*Δbtxxx*).

573

574 *Bacteroides* spp. were routinely cultured under anaerobic conditions at 37 °C using an  
575 anaerobic cabinet (Whitley A35 Workstation; Don Whitley) in culture volumes of 0.2, 2 or  
576 5 ml) of TYG (tryptone-yeast extract-glucose medium) or minimal medium (MM)<sup>31</sup> containing  
577 0.5-1% of an appropriate carbon source and 1.2 mg ml<sup>-1</sup> porcine haematin (Sigma-Aldrich)  
578 as previously described<sup>10</sup>. The growth of the cultures was monitored by OD<sub>600nm</sub> using a  
579 Biochrom WPA cell density meter for the 5 ml cultures or a Gen5 v2.0 Microplate Reader  
580 (Biotek) for the 0.2 and 2 ml cultures.

581

#### 582 **Protein cellular localization of BT0264 using antibodies**

583 Cellular localization of proteins was carried out as described previously<sup>37</sup>. In brief, *B.*  
584 *thetaiotaomicron* was grown overnight (OD<sub>600 nm</sub> value of 2.0) in 5 ml MM containing LA-  
585 AGP. The next day, cells were collected by centrifugation at 5,000g for 10 min and  
586 resuspended in 2 ml PBS. Proteinase K (0.5 mg ml<sup>-1</sup> final concentration) was added to 1 ml  
587 of the suspension and the other half left untreated (control). Both samples were incubated at  
588 37 °C for 16 h followed by centrifugation (5,000g for 10 min) to collect cells. To eliminate  
589 residual proteinase K activity, cell pellets were resuspended in 1 ml of 1.5 M trichloroacetic  
590 acid and incubated on ice for 30 min. Precipitated mixtures were then centrifuged (5,000g,  
591 10 min) and washed twice in 1 ml ice-cold acetone (99.8%). The resulting pellets were  
592 allowed to dry in a 40 °C heat block for 5 min and dissolved in 250 μl Laemmli buffer.  
593 Samples were heated for 5 min at 98 °C and mixed by pipetting several times before  
594 resolving by SDS-PAGE using 12% gels. Electrophoresed proteins were transferred to  
595 nitrocellulose membranes by western blotting followed by immunochemical detection using  
596 primary rabbit polyclonal antibodies (Eurogentec) generated against BT0264 and secondary  
597 goat anti-rabbit antibodies (Santa Cruz Biotechnology).

598

#### 599 **Proteomics**

600 **Cell surface shaving:** *Bacteriodes* cell surface digestion was performed as previously  
601 described<sup>48</sup>, with minor modifications. Briefly, *Bacteriodes* cells were harvested by  
602 centrifugation (3500 g, 15 min, 4 °C) and washed three times with PBS pH 7.4. Cell pellets  
603 were subsequently resuspended in surface shaving buffer (PBS pH 7.4 containing 0.25 M  
604 Sucrose). Surface shaving was performed using 2 μg trypsin at 37 °C for 30 min with  
605 shaking at 300 rpm. Cells in surface shaving buffer without trypsin served as controls. After  
606 surface shaving, the cells were pelleted by centrifugation (10000 g, 10 min, room  
607 temperature), and the supernatants were filter-sterilized using 0.22 μm spin filters (Corning  
608 Incorporated). Sterilized supernatants were subsequently incubated for an additional 16  
609 hours at 37 °C for complete digestion. Trypsin digestion was stopped with the addition of  
610 trifluoroacetic acid (TFA) at a final concentration of 1%, and peptides were desalted using  
611 Macro C18 Spin Columns (Harvard Apparatus).

612 **Whole-cell lysate preparation:** *Bacteriodes* cells were harvested and washed as described  
613 above. Cell pellets were subsequently resuspended in 8 M urea buffer in 50 mM  
614 triethylammonium bicarbonate (TEAB), containing 5mM tris(2-carboxyethyl)phosphine. Cells  
615 were lysed via sonication using an ultrasonic homogenizer (Hielscher). Proteins were  
616 subsequently alkylated for 30 min at room temperature using 10 mM iodoacetamide in the  
617 dark. Protein concentration was determined using a Bradford protein assay (Thermo Fisher

618 Scientific). Protein samples, containing 50 µg total protein, was diluted 5 fold with 50 mM  
619 TEAB and protein digestion was performed at 37 °C for 18 h with shaking at 300 rpm. A  
620 protein to trypsin ratio of 50:1 was used. Trypsin digestion was stopped and peptides were  
621 desalted as described above.

622 **Mass spectrometry:** Peptides were dissolved in 2% acetonitrile containing 0.1% TFA, and  
623 each sample was independently analysed on an Orbitrap Fusion Lumos Tribrid mass  
624 spectrometer (Thermo Fisher Scientific), connected to a UltiMate 3000 RSLCnano System  
625 (Thermo Fisher Scientific). Peptides were injected on an Acclaim PepMap 100 C18 LC trap  
626 column (100 µm ID × 20 mm, 3µm, 100Å) followed by separation on an EASY-Spray nanoLC  
627 C18 column (75 ID µm × 500 mm, 2µm, 100Å) at a flow rate of 300 nL/min. Solvent A was  
628 water containing 0.1% formic acid, and solvent B was 80% acetonitrile containing 0.1%  
629 formic acid. The gradient used for analysis of surface-shaved samples was as follows:  
630 solvent B was maintained at 3% for 6 min, followed by an increase from 3 to 35% B in 43  
631 min, 35-90% B in 0.5 min, maintained at 90% B for 5.4 min, followed by a decrease to 3% in  
632 0.1 min and equilibration at 3% for 10 min. The gradient used for analysis of proteome  
633 samples was as follows: solvent B was maintained at 3% for 6 min, followed by an increase  
634 from 3 to 35% B in 218 min, 35-90% B in 0.5 min, maintained at 90% B for 5 min, followed  
635 by a decrease to 3% in 0.5 min and equilibration at 3% for 10 min. The Orbitrap Fusion  
636 Lumos was operated in positive ion data-dependent mode using a modified version of the  
637 recently described CHarge Ordered Parallel Ion aNalysis (CHOPIN) method for  
638 synchronised use of both the ion trap and the Orbitrap mass analysers<sup>49</sup>. The CHOPIN  
639 method is derived from the “Universal Method” developed by Thermo Fisher, to extend the  
640 capabilities of mass analyser parallelization. The precursor ion scan (full scan) was  
641 performed in the Orbitrap in the range of 400-1600 m/z with a resolution of 120 000 at 200  
642 m/z, an automatic gain control (AGC) target of  $4 \times 10^5$  and an ion injection time of 50 ms.  
643 MS/MS spectra of doubly charged precursor ions were acquired in the linear ion trap (IT)  
644 using rapid scan mode after collision-induced dissociation (CID) fragmentation. A CID  
645 collision energy of 32% was used, the AGC target was set to  $2 \times 10^3$  and a 300 ms injection  
646 time was allowed. Precursor ions with charge state 3-7 and with an intensity  $< 5 \times 10^5$  were  
647 also scheduled for analysis by CID/IT, as described above. Precursor ions with charge state  
648 3-7 and with an intensity  $> 5 \times 10^5$  were, however, acquired in the Orbitrap (FT) with a  
649 resolution of 30 000 at 200 m/z after high-energy collisional dissociation (HCD). An HCD  
650 collision energy of 30% was used, the AGC target was set to  $1 \times 10^4$  and a 40 ms injection  
651 time was allowed. The number of MS/MS events between full scans was determined on-the-  
652 fly to maintain a 3 s fixed duty cycle. Dynamic exclusion of ions within a  $\pm 10$  p.p.m. m/z  
653 window was implemented using a 35 s exclusion duration. An electrospray voltage of 2.0 kV  
654 and capillary temperature of 275 °C, with no sheath and auxiliary gas flow, was used.

655 **Mass spectrometry data analysis:** All tandem mass spectra were analysed using  
656 MaxQuant 1.5.1.7<sup>50</sup>, and searched against a combined database of *Bacteroides*  
657 *thetaiotaomicron* VPI-5482 (containing 4782 entries), *B. cellulosilyticus* MGS:158 (containing  
658 4369 entries) and the *B. cellulosilyticus* BACCELL\_00844 glycosyl hydrolase family 16  
659 protein. Protein sequences were downloaded from Uniprot on May 10th 2018. Peak list  
660 generation was performed within MaxQuant and searches were performed using default  
661 parameters and the built-in Andromeda search engine<sup>51</sup>. The enzyme specificity was set to  
662 consider fully tryptic peptides, and two missed cleavages were allowed. Oxidation of  
663 methionine, N-terminal acetylation and deamidation of asparagine and glutamine was  
664 allowed as variable modifications. No fixed modifications were employed in searches for the  
665 surface-shaved samples, whereas carbamidomethylation of cysteine was allowed as fixed  
666 modification in proteome searches. A protein and peptide false discovery rate (FDR) of less  
667 than 1% was employed in MaxQuant. Proteins were considered confidently identified when

668 they contained at least two unique tryptic peptides. Proteins that contained similar peptides  
669 and that could not be differentiated based on tandem mass spectrometry analysis alone  
670 were grouped to satisfy the principles of parsimony. Reverse hits and contaminants were  
671 removed before downstream analysis. Skyline 4.1.0.11796 was used for extraction of ion  
672 chromatograms<sup>52</sup>. Gene ontology (Ashburner et al. 2000) enrichment was performed using  
673 PANTHER<sup>53</sup> and subcellular protein localization prediction was performed using LocateP  
674 v2<sup>54</sup>. The mass spectrometry proteomics data have been deposited to the  
675 ProteomeXchange Consortium via the PRIDE partner repository with data set identifier  
676 PXD010274.

677

### 678 **Cross-feeding and competition assays**

679 Prior to co-culture each *Bacteroides spp.* was grown in TYG and washed in PBS before  
680 being used to inoculate MM containing 0.5% GA-AGP. Co-cultures were grown in triplicate.  
681 Samples of 0.5 ml were taken at regular intervals during growth, which were serially diluted  
682 and plated onto Brain-Heart Infusion (BHI, Sigma-Aldrich) with agar and porcine hematin for  
683 determination of total CFU/ml of the culture. Mono-cultures of each *Bacteroides spp.* were  
684 also plated for determination of CFU/ml at intervals during the growth. Genomic DNA was  
685 purified from the remainder of the co-culture sample (Bacterial genomic DNA purification kit,  
686 Sigma-Aldrich). Quantitative PCR (q-PCR) was performed in triplicate on each sample using  
687 a ROCHE Lightcycler 96 to determine the ratio of each *Bacteroides spp.* and mutants in the  
688 sample using primers specific for unique regions in each *Bacteroides sp.* genome. Primers  
689 for *B. thetaiotaomicron* (F:5'-AGGTGCAGGCAACCT-3', R:5'-  
690 AATCCCGTTTCTCCATGTCC-3'); *B. ovatus* (F:5'-  
691 GGAATGAGCATAATCCATATATCAAGATGAAACG-3', R:5'-  
692 TACCTGAAACAATCATCCTTTATTTCTGTAGC-3'); *B. cellulosypticus* (F:5'-  
693 AGCAGGCGGAATTCGATAAG-3' R:5'-GTGTACAGTGCCAGGCATAA-3') and *B. caccae*  
694 (F:5'-GATTATGTGGACAGGTGATCGTGTGATTC-3', R:5'-  
695 ATTCCACCAAATGTAGGCGGGACGTTTAAT-3') were used to determine ratio of each  
696 species in co-culture and used to calculate the CFU/ml of each organisms in the culture.  
697

### 698 **Crystal structure determination**

699 **Crystallization:** BT0290-E182A at 10 mg/ml, was crystallized from the commercial screen  
700 Morpheus (Molecular Dimensions, UK) condition D3 (20 mM 1,6-Hexanediol, 20 mM 1-  
701 Butanol, 20 mM 1,2-Propanediol (racemic), 20 mM 2-Propanol, 20 mM 1,4-Butanediol, 20  
702 mM 1,3-Propanediol, 100 mM Imidazole-MES pH 6.5, 30% Glycerol and 30% polyethylene  
703 glycol 4000). Apo BT0265 was crystallised at 32 mg/ml in 20% PEG 3350 and 0.2 M  
704 Sodium/Potassium Tartrate. Crystals were cryoprotected with 20 % glycerol. Crystals of  
705 BT0265 Q249A were crystallised at 20 mg/ml, with a 200mg/ml oligosaccharide mixture, in  
706 20 % PEG 3350 and 0.2 M sodium thiocyanate. Crystals were cryo protected with paratone  
707 oil.

708 BT3683 was crystallised at 12.6 mg/ml in 20 % PEG 3350, 0.2 M Ammonium formate and  
709 300 mM L-rhamnose. Crystals formed under these conditions were then back soaked, in  
710 mother liquor overnight to remove the rhamnose. These crystals were then transferred to a  
711 fresh drop and soaked with galactose, galactodeoxynorijmycin or galactimidazole, as  
712 desired, at concentrations in >30 mM. These crystals were left overnight and then cryo  
713 protected with paratone oil.

714

715

716 **Data collection and processing:** Diffraction data for BT0290 and BT3674 were collected at  
717 the Diamond Light Source, U.K., on beamline I02, whilst, all other data was collected on  
718 bealine IO4-1, at a temperature of 100 °K. All data were processed and integrated with XDS  
719 and scaled using Aimless<sup>38, 39</sup>. For all datasets, the space groups were determined using  
720 pointless and later confirmed during refinement<sup>40</sup>. The phase problem was solved by  
721 molecular replacement using Phaser<sup>41</sup>. PDB 3D3A was used as search model for BT0290;  
722 BT3674 was solved using 4QJY; BT0265 was solved using 3VSF and a truncated version of  
723 BT0265, lacking the C-terminal Ig domain was used to solve BT3683. Additional automated  
724 model building for BT0265 was carried out using buccaneer<sup>42</sup>. Solvent molecules were  
725 added using COOT<sup>43</sup> and checked manually. All other computing used the CCP4 suite of  
726 programs<sup>44</sup>. Five percent of the observations were randomly selected for the Rfree set. The  
727 models were validated using Molprobrity<sup>45</sup>. The data statistics and refinement details are  
728 reported in **Supplementary Table 6**.

729

### 730 **Comparative genomics analysis**

731 Using a similar strategy to the identification pectin PULs, AGP PULs were searched for in  
732 Bacteroidetes genomes. The identification of similar PULs was based on PUL alignments.  
733 Gene composition and order of Bacteroidetes PULs were computed using the PUL predictor  
734 described in PULDB<sup>46</sup>. Then, in a manner similar to amino acid sequence alignments, the  
735 predicted PULs were aligned to the appropriate pectin PULs according to their modularity as  
736 proposed in the RADS/RAMPAGE method<sup>47</sup>. Modules taken into account include CAZy  
737 families, sensor-regulators and *suscd*-like genes. Finally, PUL boundaries and limit cases  
738 were refined by BLASTP-based analysis. The glycoside hydrolase families discovered in this  
739 study are listed in the main text.

740

741 **Data availability.** The data that support the findings of this study are available from  
742 the corresponding author upon request. The authors declare that the data supporting the  
743 findings of this study are available within the paper and the Supplementary Information. The  
744 crystal structure datasets generated (coordinate files and structure factors) have been  
745 deposited in the Protein Data Bank (PDB) and are listed in **Supplementary Table 6** together  
746 with the PDB accession codes.

747

### 748 **REFERENCES**

749

- 750 1. Clemente, J.C., Ursell, L.K., Parfrey, L.W. & Knight, R. The impact of the gut  
751 microbiota on human health: an integrative view. *Cell* **148**, 1258-1270 (2012).
- 752 2. El Kaoutari, A., Armougom, F., Gordon, J.I., Raoult, D. & Henrissat, B. The  
753 abundance and variety of carbohydrate-active enzymes in the human gut microbiota.  
754 *Nat Rev Microbiol* **11**, 497-504 (2013).
- 755 3. Koropatkin, N.M., Cameron, E.A. & Martens, E.C. How glycan metabolism shapes  
756 the human gut microbiota. *Nat Rev Microbiol* **10**, 323-335 (2012).
- 757 4. Porter, N.T. & Martens, E.C. The Critical Roles of Polysaccharides in Gut Microbial  
758 Ecology and Physiology. *Annu Rev Microbiol* **71**, 349-369 (2017).
- 759 5. Gilbert, H.J., Stalbrand, H. & Brumer, H. How the walls come crumbling down: recent  
760 structural biochemistry of plant polysaccharide degradation. *Curr Opin Plant Biol* **11**,  
761 338-348 (2008).
- 762 6. Lombard, V., Golaconda Ramulu, H., Drula, E., Coutinho, P.M. & Henrissat, B. The  
763 carbohydrate-active enzymes database (CAZy) in 2013. *Nucleic Acids Res* **42**, D490-  
764 495 (2014).
- 765 7. Davies, G. & Henrissat, B. Structures and mechanisms of glycosyl hydrolases.  
766 *Structure* **3**, 853-859 (1995).
- 767 8. Ndeh, D. & Gilbert, H.J. Biochemistry of complex glycan depolymerisation by the  
768 human gut microbiota. *FEMS Microbiol Rev* **42**, 146-164 (2018).

- 769 9. Martens, E.C., Koropatkin, N.M., Smith, T.J. & Gordon, J.I. Complex glycan  
770 catabolism by the human gut microbiota: the Bacteroidetes Sus-like paradigm. *J Biol*  
771 *Chem* **284**, 24673-24677 (2009).
- 772 10. Larsbrink, J. et al. A discrete genetic locus confers xyloglucan metabolism in select  
773 human gut Bacteroidetes. *Nature* **506**, 498-502 (2014).
- 774 11. Luis, A.S. et al. Dietary pectic glycans are degraded by coordinated enzyme  
775 pathways in human colonic Bacteroides. *Nat Microbiol* **3**, 210-219 (2018).
- 776 12. Fincher, G.B., Stone, B.A. & Clarke, A.E. Arabinogalactan-Proteins - Structure,  
777 Biosynthesis, and Function. *Annu Rev Plant Phys* **34**, 47-70 (1983).
- 778 13. Vidal, S., Williams, P., Doco, T., Moutounet, M. & Pellerin, P. The polysaccharides of  
779 red wine: total fractionation and characterization. *Carbohydr Polym* **54**, 439-447  
780 (2003).
- 781 14. Capek, P., Matulova, M., Navarini, L. & Suggi-Liverani, F. Structural features of an  
782 arabinogalactan-protein isolated from instant coffee powder of Coffea arabica beans  
783 *Carbohydr. Polym.* **80**, 180-185 (2010).
- 784 15. Dauqan, E. & Abdullah, A. Utilization of gum arabic for industries and human health.  
785 *American Journal of Applied Sciences* **10**, 1270-1279 (2013).
- 786 16. McNamara, M.K. & Stone, B.A. Isolation, characterization and chemical synthesis of  
787 a galactosyl-hydroxyproline linkage compound from wheat endosperm  
788 arabinogalactan-peptide. *Lebensm. Wiss. Technol.* **14**, 182-187 (1981).
- 789 17. Ichinose, H. et al. Characterization of an exo-beta-1,3-galactanase from *Clostridium*  
790 *thermocellum*. *Appl Environ Microbiol* **72**, 3515-3523 (2006).
- 791 18. Munoz-Munoz, J. et al. An evolutionarily distinct family of polysaccharide lyases  
792 removes rhamnose capping of complex arabinogalactan proteins. *J Biol Chem* **292**,  
793 13271-13283 (2017).
- 794 19. Munoz-Munoz, J., Cartmell, A., Terrapon, N., Henrissat, B. & Gilbert, H.J. Unusual  
795 active site location and catalytic apparatus in a glycoside hydrolase family. *Proc Natl*  
796 *Acad Sci U S A* **114**, 4936-4941 (2017).
- 797 20. Calame, W., Weseler, A.R., Viebke, C., Flynn, C. & Siemensma, A.D. Gum arabic  
798 establishes prebiotic functionality in healthy human volunteers in a dose-dependent  
799 manner. *Br J Nutr* **100**, 1269-1275 (2008).
- 800 21. Martens, E.C. et al. Recognition and degradation of plant cell wall polysaccharides by  
801 two human gut symbionts. *PLoS Biol* **9**, e1001221 (2011).
- 802 22. Mewis, K., Lenfant, N., Lombard, V. & Henrissat, B. Dividing the Large Glycoside  
803 Hydrolase Family 43 into Subfamilies: a Motivation for Detailed Enzyme  
804 Characterization. *Appl Environ Microbiol* **82**, 1686-1692 (2016).
- 805 23. Kotake, T. et al. Endo-beta-1,3-galactanase from winter mushroom *Flammulina*  
806 *velutipes*. *J Biol Chem* **286**, 27848-27854 (2011).
- 807 24. Cartmell, A. et al. The structure and function of an arabinan-specific alpha-1,2-  
808 arabinofuranosidase identified from screening the activities of bacterial GH43  
809 glycoside hydrolases. *J Biol Chem* **286**, 15483-15495 (2011).
- 810 25. Kitazawa, K. et al. beta-galactosyl Yariv reagent binds to the beta-1,3-galactan of  
811 arabinogalactan proteins. *Plant Physiol* **161**, 1117-1126 (2013).
- 812 26. Nakamura, A. et al. "Newton's cradle" proton relay with amide-imidic acid  
813 tautomerization in inverting cellulase visualized by neutron crystallography. *Science*  
814 *Advances* **1** (2015).
- 815 27. Gloster, T.M., Turkenburg, J.P., Potts, J.R., Henrissat, B. & Davies, G.J. Divergence  
816 of catalytic mechanism within a glycosidase family provides insight into evolution of  
817 carbohydrate metabolism by human gut flora. *Chem Biol* **15**, 1058-1067 (2008).
- 818 28. Rakoff-Nahoum, S., Coyne, M.J. & Comstock, L.E. An ecological network of  
819 polysaccharide utilization among human intestinal symbionts. *Current biology : CB*  
820 **24**, 40-49 (2014).
- 821 29. Rakoff-Nahoum, S., Foster, K.R. & Comstock, L.E. The evolution of cooperation  
822 within the gut microbiota. *Nature* **533**, 255-259 (2016).



- 823 30. Cartmell, A. et al. How members of the human gut microbiota overcome the sulfation  
824 problem posed by glycosaminoglycans. *Proc Natl Acad Sci U S A* **114**, 7037-7042  
825 (2017).
- 826 31. Sharma, S.K., Corrales, G. & Penadés, S. Single Step Stereoselective Synthesis of  
827 Unprotected 2,4-Dinitrophenyl Glycosides, . *Tetrahedron Lett* **36**, 5627-5630 (1995).
- 828 32. Vonhoff, S., Heightman, T.D. & Vasella, A. Inhibition of glycosidases by lactam  
829 oximes: Influence of the aglycon in disaccharide analogues. *Helvetica Chimica Acta*  
830 **81**, 1710-1725 (1998).
- 831 33. Cavanagh, J., Fairbrother, W.J., Palmer, A.G. & Skelton, N.J. Protein NMR  
832 Spectroscopy: Principles and Practice. (Academic Press, San Diego, CA, USA;  
833 1996).
- 834 34. Vranken, W.F. et al. The CCPN data model for NMR spectroscopy: development of a  
835 software pipeline. *Proteins* **59**, 687-696 (2005).
- 836 35. Bock, K. & Pedersen, C. Study of CH-13 coupling-constants in pentapyranoses and  
837 some of their derivatives. *Acta Chemica Scandinavica Series B-Organic Chemistry*  
838 *and Biochemistry* **B 29**, 258-264 (1975).
- 839 36. Koropatkin, N.M., Martens, E.C., Gordon, J.I. & Smith, T.J. Starch catabolism by a  
840 prominent human gut symbiont is directed by the recognition of amylose helices.  
841 *Structure* **16**, 1105-1115 (2008).
- 842 37. Cuskin, F. et al. Human gut Bacteroidetes can utilize yeast mannan through a selfish  
843 mechanism. *Nature* **517**, 165-169 (2015).
- 844 38. Evans, P.R. An introduction to data reduction: space-group determination, scaling  
845 and intensity statistics. *Acta crystallographica. Section D, Biological crystallography*  
846 **67**, 282-292 (2011).
- 847 39. Kabsch, W. XDS. *Acta Crystallographica Section D-Biological Crystallography* **66**,  
848 125-132 (2010).
- 849 40. Evans, P. Scaling and assessment of data quality. *Acta crystallographica. Section D,*  
850 *Biological crystallography* **62**, 72-82 (2006).
- 851 41. McCoy, A.J. et al. Phaser crystallographic software. *J Appl Crystallogr.* **40**, 658-674  
852 (2007).
- 853 42. Cowtan, K. The Buccaneer software for automated model building. 1. Tracing protein  
854 chains. *Acta crystallographica. Section D, Biological crystallography* **62**, 1002-1011  
855 (2006).
- 856 43. Emsley, P., Lohkamp, B., Scott, W.G. & Cowtan, K. Features and development of  
857 Coot. *Acta crystallographica. Section D, Biological crystallography* **66**, 486-501  
858 (2010).
- 859 44. Winn, M.D. et al. Overview of the CCP4 suite and current developments. *Acta*  
860 *Crystallographica Section D-Biological Crystallography* **67**, 235-242 (2011).
- 861 45. Chen, V.B. et al. MolProbity: all-atom structure validation for macromolecular  
862 crystallography. *Acta crystallographica. Section D, Biological crystallography* **66**, 12-  
863 21 (2010).
- 864 46. Terrapon, N., Lombard, V., Gilbert, H.J. & Henrissat, B. Automatic prediction of  
865 polysaccharide utilization loci in Bacteroidetes species. *Bioinformatics* **31**, 647-655  
866 (2015).
- 867 47. Terrapon, N., Weiner, J., Grath, S., Moore, A.D. & Bornberg-Bauer, E. Rapid  
868 similarity search of proteins using alignments of domain arrangements.  
869 *Bioinformatics* **30**, 274-281 (2014).
- 870 48. Rodriguez-Ortega, M. J. et al. Characterization and identification of vaccine  
871 candidate proteins through analysis of the group A Streptococcus surface proteome.  
872 *Nat Biotechnol* **24**, 191-197 (2006).
- 873 49. Davis, S. et al. Expanding Proteome Coverage with CHarge Ordered Parallel Ion  
874 aNalysis (CHOPIN) Combined with Broad Specificity Proteolysis. *J Proteome Res*  
875 **16**, 1288-1299 (2017).

- 876 50. Cox, J. & Mann, M. MaxQuant enables high peptide identification rates,  
877 individualized p.p.b.-range mass accuracies and proteome-wide protein  
878 quantification. *Nat Biotechnol* **26**, 1367-1372 (2008).
- 879 51. Cox, J. *et al.* Andromeda: a peptide search engine integrated into the MaxQuant  
880 environment. *J Proteome Res* **10**, 1794-1805 (2011).
- 881 52. MacLean, B. *et al.* Skyline: an open source document editor for creating and  
882 analyzing targeted proteomics experiments. *Bioinformatics* **26**, 966-968 (2010).
- 883 53. Mi, H. *et al.* PANTHER version 11: expanded annotation data from Gene Ontology  
884 and Reactome pathways, and data analysis tool enhancements. *Nucleic Acids Res*  
885 **45**, D183-D189 (2017).
- 886 54. Zhou, M., Boekhorst, J., Francke, C. & Siezen, R. J. LocateP: genome-scale  
887 subcellular-location predictor for bacterial proteins. *BMC Bioinformatics* **9**, 173  
888 (2008).

889

890 **Correspondence and requests for materials should be addressed to H.J.G.**

### 891 **Acknowledgements**

892 This work was supported in part by an Advanced Grant from the European Research  
893 Council (Grant No. 322820) awarded to H.J.G. and B.H. supporting D.N., A.C., J. M.-M.,  
894 J.B., N.T., a Wellcome Trust Senior Investigator Award to HJG (grant No. WT097907MA)  
895 that supported E.C.L. The Biotechnology and Biological Research Council project "Ricefuel"  
896 (grant numbers BB/K020358/1) awarded to H.J.G. supported A.L. We thank Diamond Light  
897 Source for access to beamline I02, I04-1 and I24 (mx1960, mx7854 and mx9948) that  
898 contributed to the results presented here.

899

900 **Conflict of interest:** The authors declare that they have no conflicts of interest with the  
901 contents of this article

902

### 903 **Author contributions**

904 Enzyme characterisation and oligosaccharide purification were by A.C., D.N. and J.M.-M.  
905 Gene deletion strains were constructed by D.N. and A.L. Co-culturing experiments were  
906 carried out by J.B. and D.N. Western blots were by D.N. Phylogenetic reconstruction and  
907 metagenomic analysis were by N.T. and B.H. Bacterial growth and transcriptomic  
908 experiments: E.C.L. and D.N. X-ray protein crystallography was by A.C., A.B. J.M.-M.  
909 N.M.R. experiments were by A.C. and K.S. Mass spectrometry was by J.G., L.Y. and P.D.  
910 Chemical synthesis was by P.Z.F., S.S. and S.J.W. E.H., M.T. and E.C.L. performed the  
911 whole cell proteomics. Experiments were designed by H.J.G. A.C. J.M.-M. and D.N. The  
912 manuscript was written by H.J.G. with substantial contributions from N.T., B.H. and S.J.W.  
913 Figures were prepared by J.M.-M. and E.C.L.

914

915

916

917

918

919

920

921

922

923

924

925

926

927 **FIGURE LEGENDS**

928

929 **Figure 1. The structure of arabinogalactans, PULs upregulated by the glycans and**  
930 **enzymes that attack these glycans.** Structure of **a**, larch wood (LA-AGP) and **b**, gum  
931 arabic (GA-AGP) arabinogalactans, and the enzymes that act on these glycans. The  
932 enzymes are identified by their locus tag (BTXXXX and BaccellXXXX are derived from *B.*  
933 *thetaitoaomicron* and *B. cellulosityticus*, respectively), assignment to cazy families (GHXX  
934 and PLXX indicate glycoside hydrolase and polysaccharide lyase families, respectively) and  
935 their predicted cellular location (based on the nature of the signal peptide and, in some  
936 cases, cellular location for the observed activity, proteomic analysis or resistance to  
937 proteinase K; see **Fig. 5aef**), in which superscript P and C indicate periplasmic and  
938 cytoplasmic location, respectively. The black arrows show the linkage  
939 cleaved by the enzymes, although the polysaccharide lyase activity of BT0263 is not  
940 functionally relevant as it is located in the cytoplasm. We propose that the  $\beta$ -L-  
941 arabinofuranose targeted by BT3674 is linked to the  $\beta$ 1,3-galactan backbone at O2 or O4.  
942 This assumption is based on the observation that the enzyme potentiates the exo- $\beta$ -1,3-  
943 galactosidases that sequentially remove galactose units from the backbone (see **Fig. 2a**).  
944 These galactosidases can target galactose residues decorated at O6 but not at O2 or O4. **c**,  
945 Schematic of *B. thetaitoaomicron* polysaccharide utilization loci (PULs) upregulated by  
946 arabinogalactan degradation.

947

948 **Figure 2 HPAEC analysis of the activity of GH43\_24  $\beta$ 1,3-D-galactanases** The AGPs  
949 were at 5 mg/ml for all reactions except BT0264 against LA-AGP and BT3683 against GA-  
950 AGP, when substrate concentration was increased to 25 mg/ml, the  $\beta$ -1,3-galactan  
951 backbone was at 1.5 mg/ml. Enzyme concentration was 1  $\mu$ M. Reactions were incubated for  
952 16 h in 20 mM sodium phosphate buffer pH 7.0 containing 150 mM NaCl buffer. The data  
953 shown are representative of three independent replicates. **a**, reveals how the GH127  $\beta$ -L-  
954 arabinofuranosidase BT3674 acts in synergy with the exo- $\beta$ 1,3-galactosidases BT0265 and  
955 BT3683 on LA-AGP. The synergy between the endo- $\beta$ 1,3-galactanase with BT0265 and  
956 BT3683 acting on LA-AGP and GA-AGP was shown in **b** and **c**, respectively. **d**, shows a  
957 time course of BT0264 acting on  $\beta$ -1,3-galactan. Peaks containing a defined  
958 galactooligosaccharide are identified by a yellow circle with the degree of polymerization  
959 shown in subscript. In **b** and **c** the peaks corresponding to  $\beta$ 1,6-galactobiose and  $\beta$ 1,6-  
960 galactotriose were identified by LC-MS (see **Supplementary Fig. 1d**), and the  $\beta$ 1,6 linkage  
961 was revealed by sensitivity to the  $\beta$ 1,6-galactosidase BT0290.

962

963 **Figure 3. The crystal structure of GH43\_24  $\beta$ 1,3-D-galactosidases in complex with**  
964 **ligands.** **a**, schematic of BT0265 (left) and BT3683 (right) in which the catalytic domains are  
965 colour ramped from *blue* at the N-terminus to *red* at the C-terminus. The C-terminal  $\beta$ -  
966 sandwich domain in BT0265 is coloured cyan. **b**, shows the solvent exposed surface of  
967 BT0265 in complex with the heptasaccharide shown in **Supplementary Fig. 3** (terminal  $\alpha$ -  
968 Gal and  $\alpha$ -Rha are not visible). Electron density for the terminal  $\alpha$ -Gal was too weak to  
969 model the sugar. The red dashes show the polar interactions between the ligand and both  
970 side chains and backbone N and O. Residues that make polar contacts with the side chain  
971 of the ligand are also shown. **c**, an overlay of the residues in BT0265 (*cyan*), BT3683 (*green*)  
972 and the GH43\_24  $\beta$ 1,3-galactosidase Cthe\_1271 (*grey*; PDB code 3VSZ) that interact with  
973 galactose (*yellow*) in complex with BT3683. **d**, BT3683 in complex with galactose (Gal),  
974 deoxygalactonojirimycin (DGJ) and galactose-imidazole (Gal-Im). Direct polar interactions  
975 between enzyme and ligand are indicated by *black* dashes and the indirect water-mediated  
976 hydrogen bonds in *magenta* dashes. The *red* dashed line represents the polar interaction  
977 between the catalytic acid (Glu520) and Ser487. The two conformations of Glu520 in the  
978 Gal-Im complex is denoted by a and b.

979

980

981 **Figure 4. Degradation of GA-AGP side chains.** The pentasaccharide substrate shown in a  
982 grey box was released from GA-AGP by the exo- $\beta$ 1,3-galactosidase BT0265 and then  
983 purified by size exclusion chromatography. Individual *B. thetaiotaomicron* enzymes (1  $\mu$ M)  
984 were incubated with the glycan (5 mM) for 16 h at 37 °C in 20 mM sodium phosphate buffer,  
985 pH 7.0. Monosaccharides and oligosaccharides generated were identified by HPAEC-PAD.  
986 The data in **a** and **b** show that the pentasaccharide could be degraded by the enzymes that  
987 comprise the LU and RG pathways, respectively. Note that the enzymes in the two pathways  
988 Verification of the degradative pathway was achieved by reconstituting the pathway using  
989 the only functioned in the order shown in the figure. The example is representative of  
990 independent replicates ( $n = 3$ ).

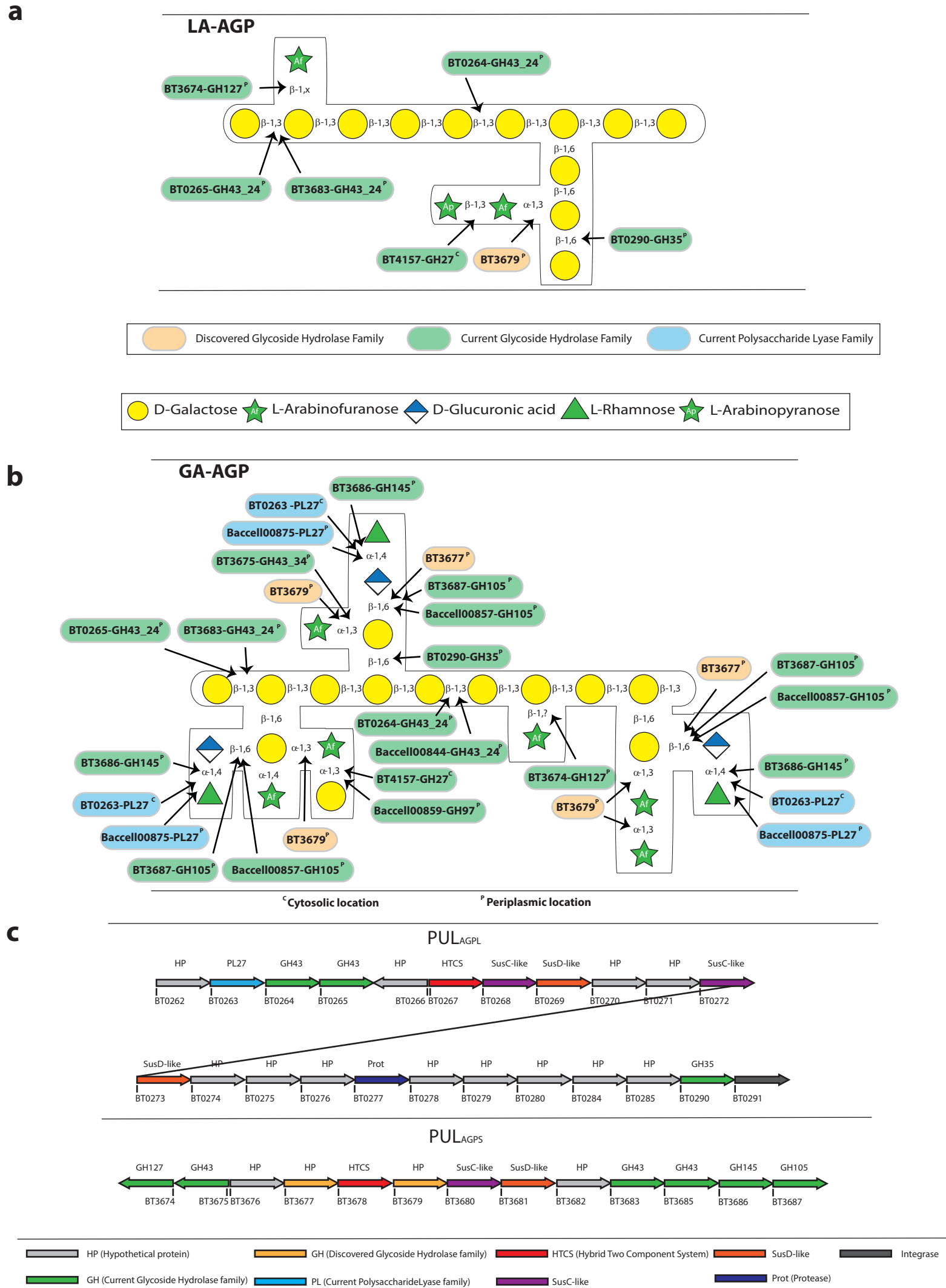
991  
992

993 **Figure 5 Cell localization and growth of *Bacteroides* on complex AGPs.** **a**, Western blot  
994 detection of BT0264 and a known surface enzyme (BT4662)<sup>30</sup> in LA-AGP/heparin cultured  
995 *B. thetaiotaomicron* after treatment of the bacterial cells with proteinase K (PK+) or untreated  
996 (PK-). Purified recombinant BT0264 was also subjected to proteinase treatment to verify the  
997 enzyme is sensitive to the proteinase. The data show that the enzyme is resistant to the  
998 proteinase and thus is not located on the cell surface. The blot is an example of biological  
999 replicates where  $n=3$ . Wild type *B. thetaiotaomicron* (Bt) and *B. thetaiotaomicron* expressing  
1000 Baccell00844 (Bt::Baccell00844) were cultured in 0.2 ml of minimal medium containing  
1001 AGPs under anaerobic conditions. **b**, growth was assessed on GA-AGP and GA-AGP pre-  
1002 treated with BT0264 [GA-AGP(BT0264)] or Baccell00844 [GA-AGP(Baccell00844)]. In **c**  
1003 growth was evaluated on wheat AGP (WH-AGP). In **b** and **c** error bars report standard  
1004 errors of the mean of biological replicates ( $n = 4$ ). **d**, HPAEC analysis of the products  
1005 generated by recombinant Baccell00844 (1  $\mu$ M) incubated with  $\beta$ -1,3-galactan for 16 h using  
1006 standard conditions. The chromatographs are examples of biological replicates ( $n = 2$ ). **e**,  
1007 Bt, Bt::Baccell00844 and *B. cellulosilyticus* (Baccell) cells derived from cultured grown on  
1008 GA-AGP were incubated with 0.5%  $\beta$ 1,3-galactan for 16 h in phosphate buffered saline  
1009 in aerobic conditions for 16 h. Under these conditions substrate is only available to  
1010 the surface enzymes. Products released from the glycan was evaluated by TLC. The  
1011 example is from biological replicates  $n = 3$ . **f**, Venn diagram of the number of proteins  
1012 identified in the surfome, the surfome and total proteome, and total proteome. Baccell00844  
1013 was unique to the surfome fraction. The 46 proteins detected only in the surfome are  
1014 described in **Supplementary Table 5**.

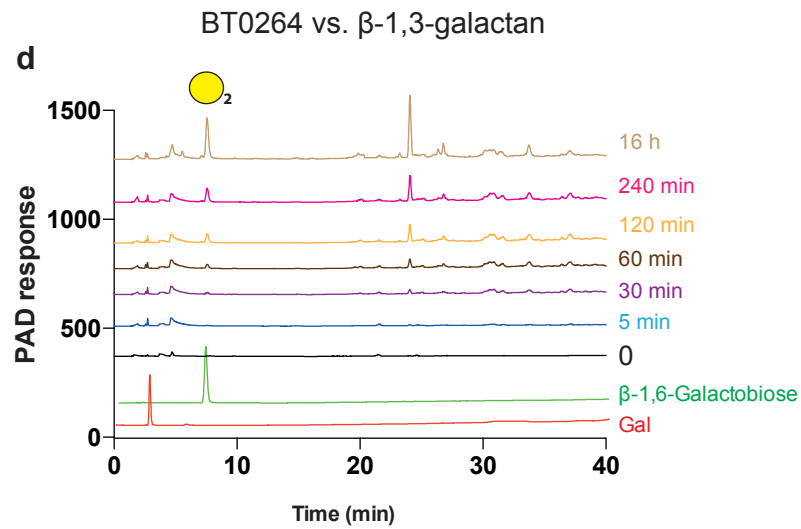
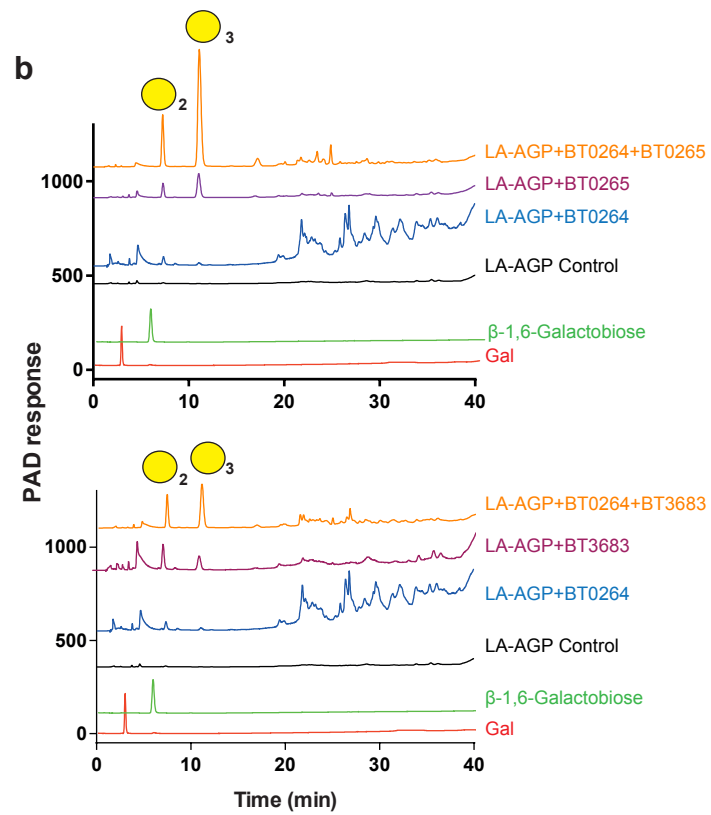
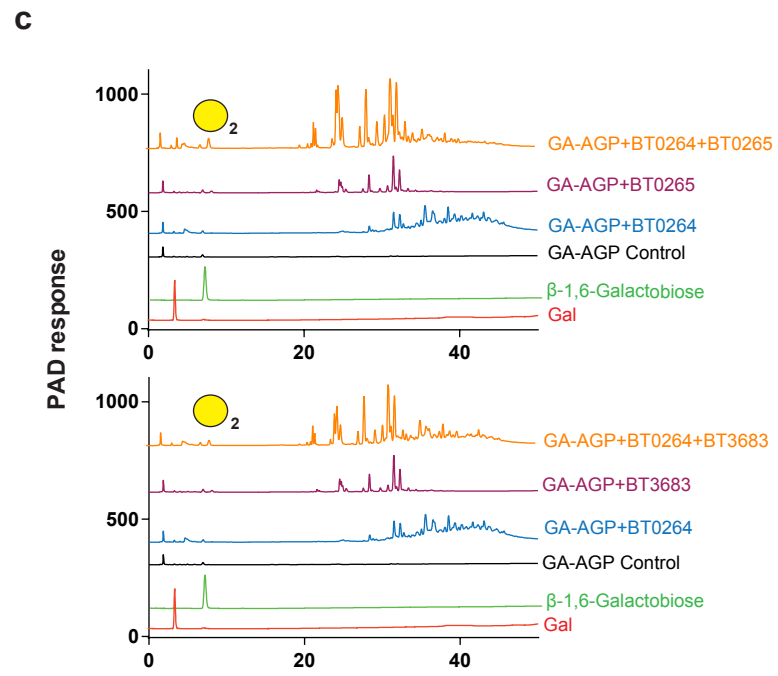
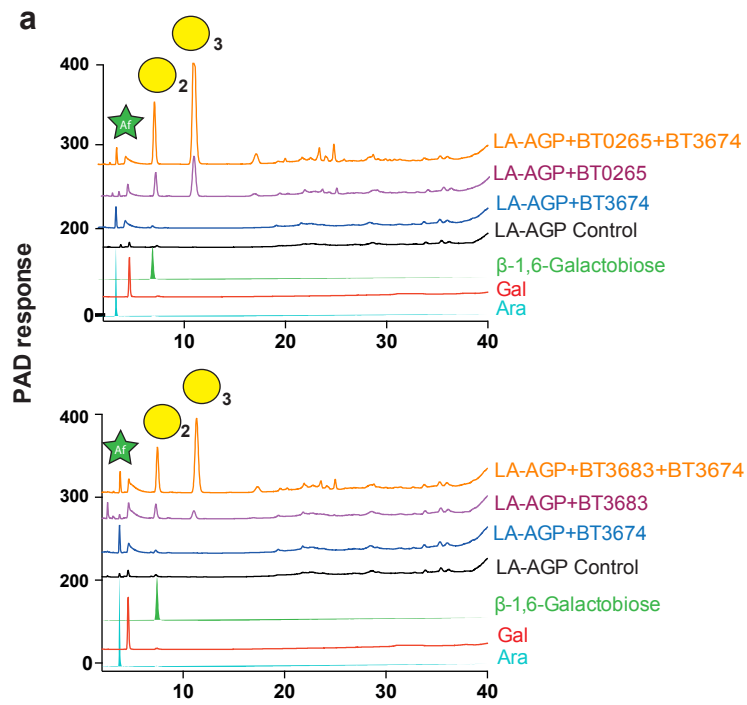
1015  
1016

1017 **Figure 6. Growth profile of keystone and recipient *Bacteroides* species on complex**  
1018 **AGPs.** Wild type *B. thetaiotaomicron* strain VPI-5482 (Bt), *B. thetaiotaomicron* strain VPI-  
1019 5482 expressing Baccell00844 (Bt::Baccell00844), *B. ovatus* strain ATCC8483 (Bo), *B.*  
1020 *cellulosilyticus* strain DSM14838 (Baccell) and *B. caccae* strain ATCC 43185 (Bcacc) were  
1021 cultured on nutrient rich (TYG) media overnight. The organisms were then inoculated at  $\sim 10^7$   
1022 colony forming units (CFUs) per ml into minimal medium containing GA-AGP at 0.5% (w/v),  
1023 either as a monoculture or in co-culture with one of the other strains. The cultures were  
1024 incubated in anaerobic conditions and at regular intervals aliquots were removed and plated  
1025 onto rich (BHI) agar plates to determine the CFUs. The ratio of the strains in the co-cultures  
1026 were determined by quantitative-PCR with primers that amplify genomic sequences unique  
1027 to each strain (see Methods for further details). **(i)** shows the ratio of the organisms in the  
1028 co-cultures and **(ii)** the corresponding CFUs for these bacterial strains. Continuous lines  
1029 correspond to organisms in co-culture and broken lines are monocultures of the bacterial  
1030 strains. **a**, Bo and Bt; **b**, Bo and Baccell; **c**, Bo and Bcacc; **d**, Baccell and Bt; **e**, Bcacc and  
1031 Bt; **f**, Bo and Bt::Baccell00844. Error bars represent the s.e.m of biological replicates ( $n=3$ ).

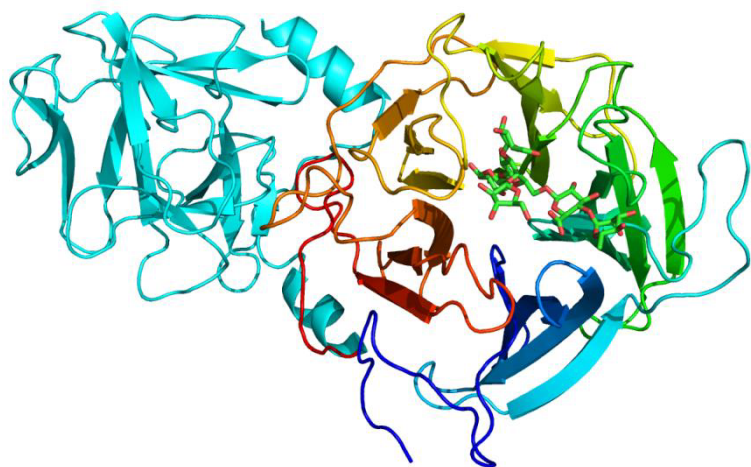
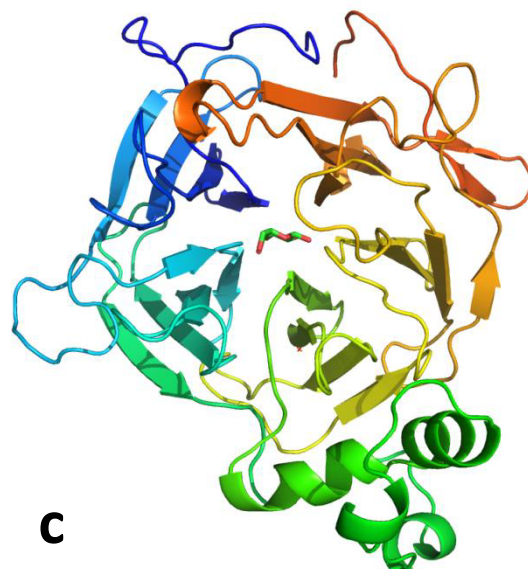
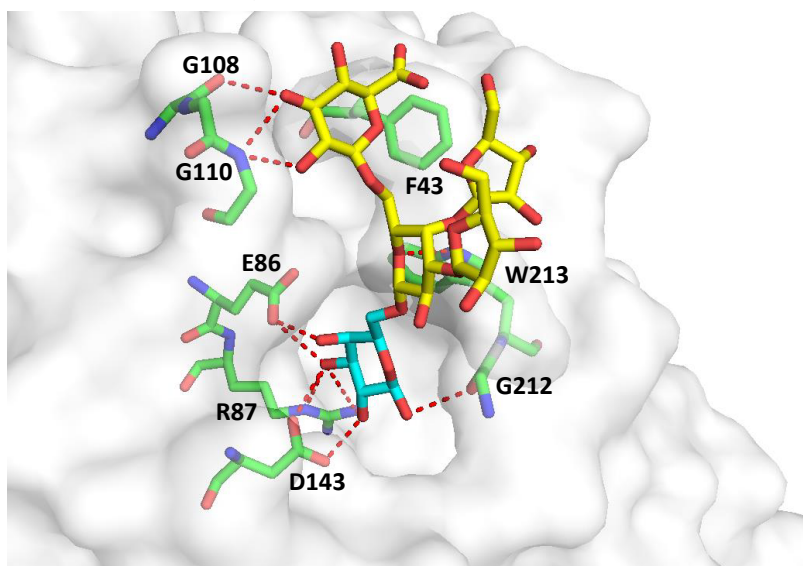
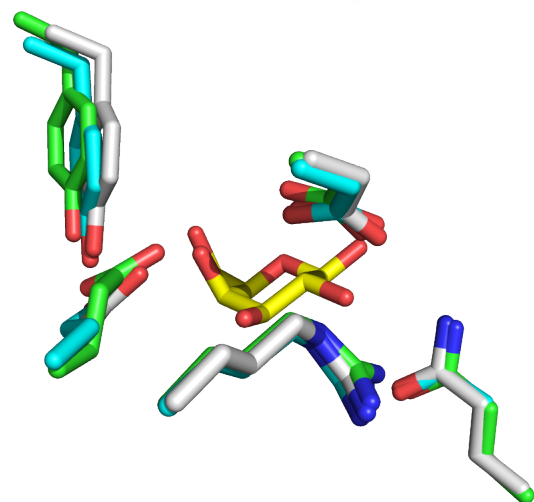
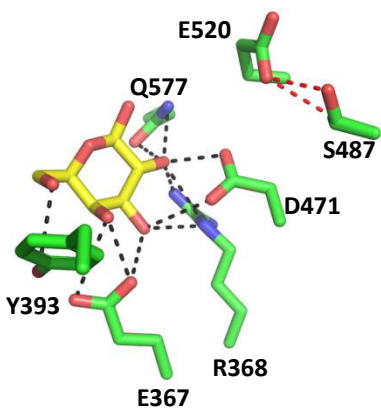
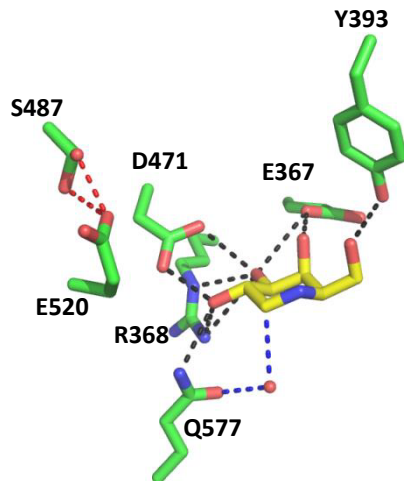
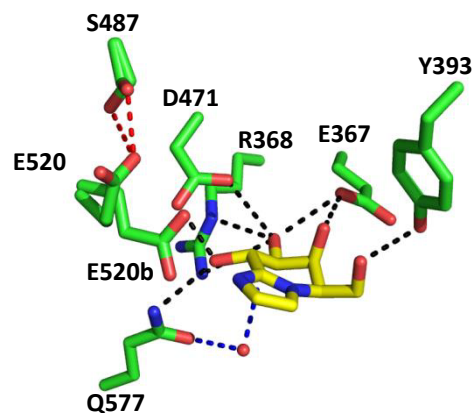
1032



**Fig. 1**



**Fig. 2**

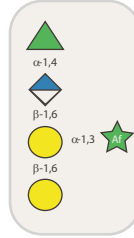
**Fig. 3****a****BT0265****BT3683****b****BT0265-Heptasaccharide****c****d****BT3683-Gal****BT3683-DNJ****BT3683-Gal-Im**





**a**  
Lyase Pathway  
(LU)

**BT0263**



**BT3686**

**b**  
Rhamno-glucuronidase  
Pathway (RG)

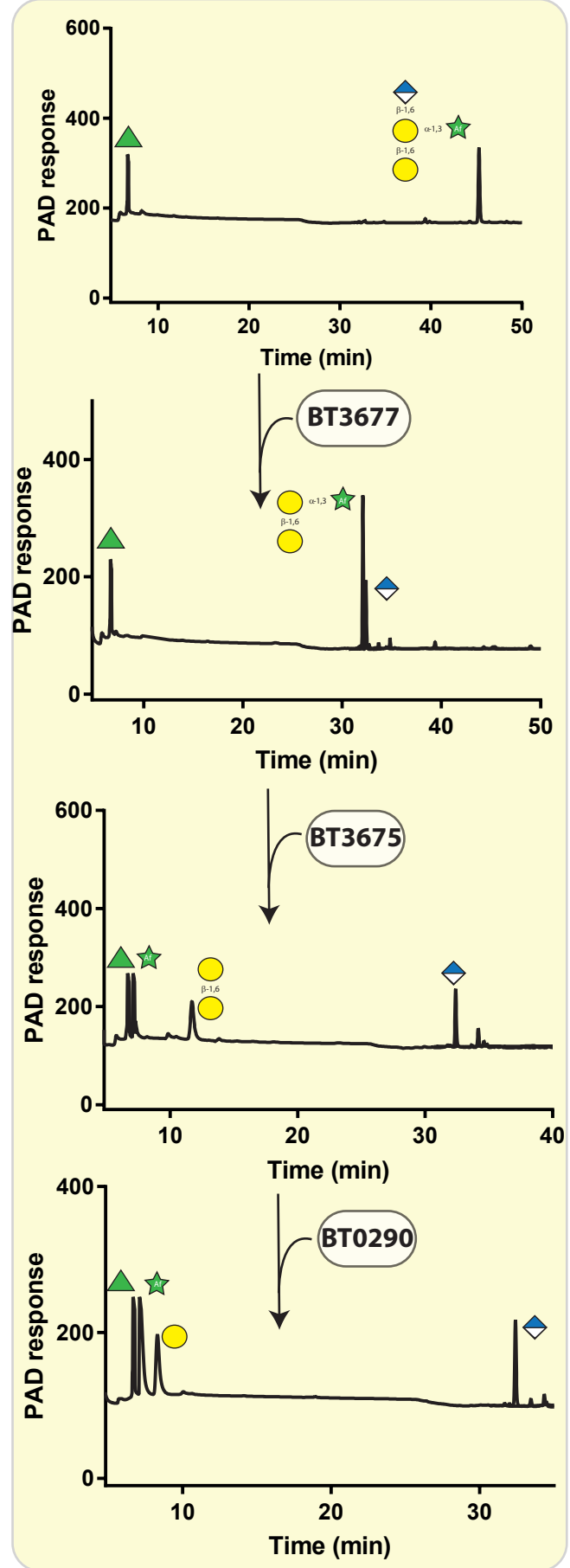
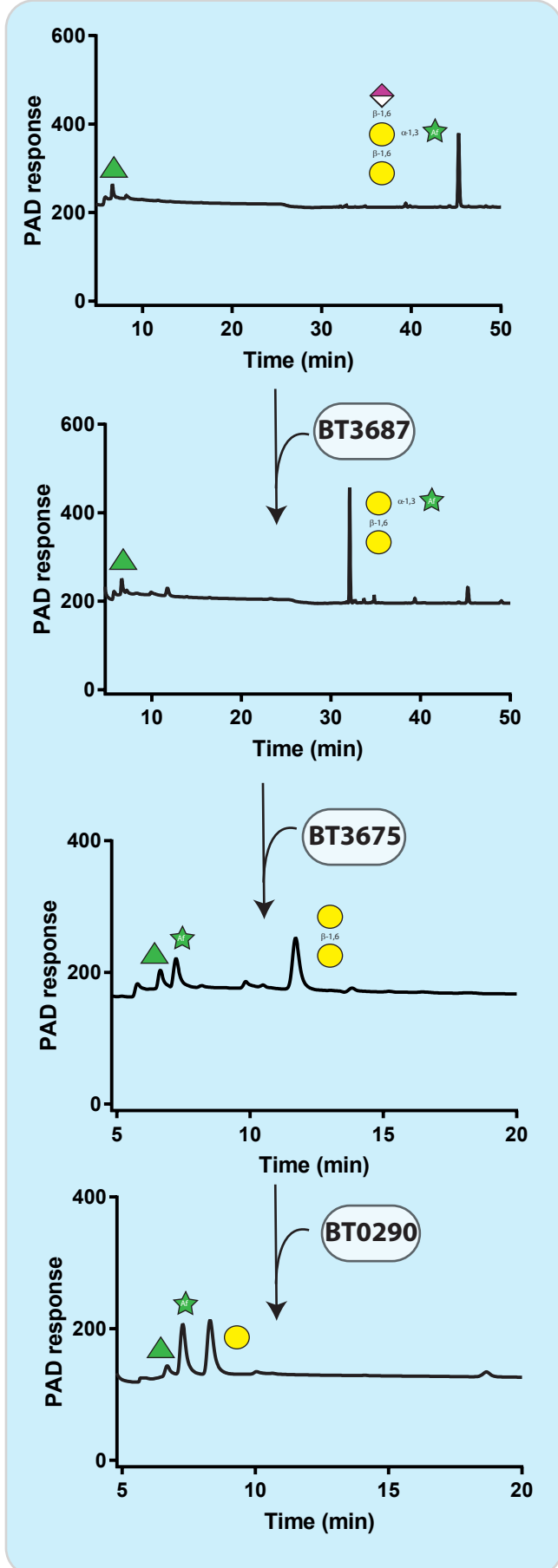


**Fig. 4**



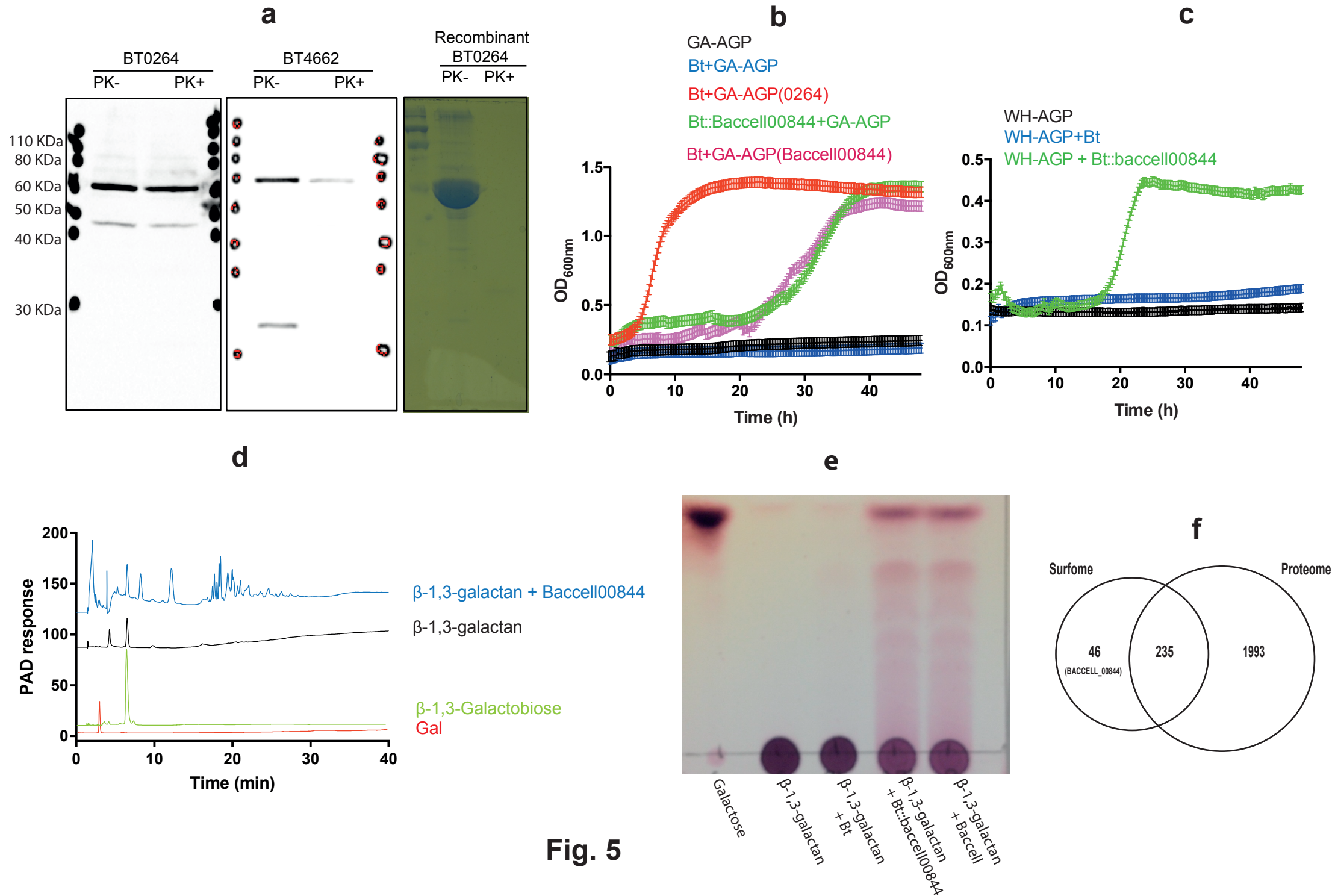


**Fig. 5**

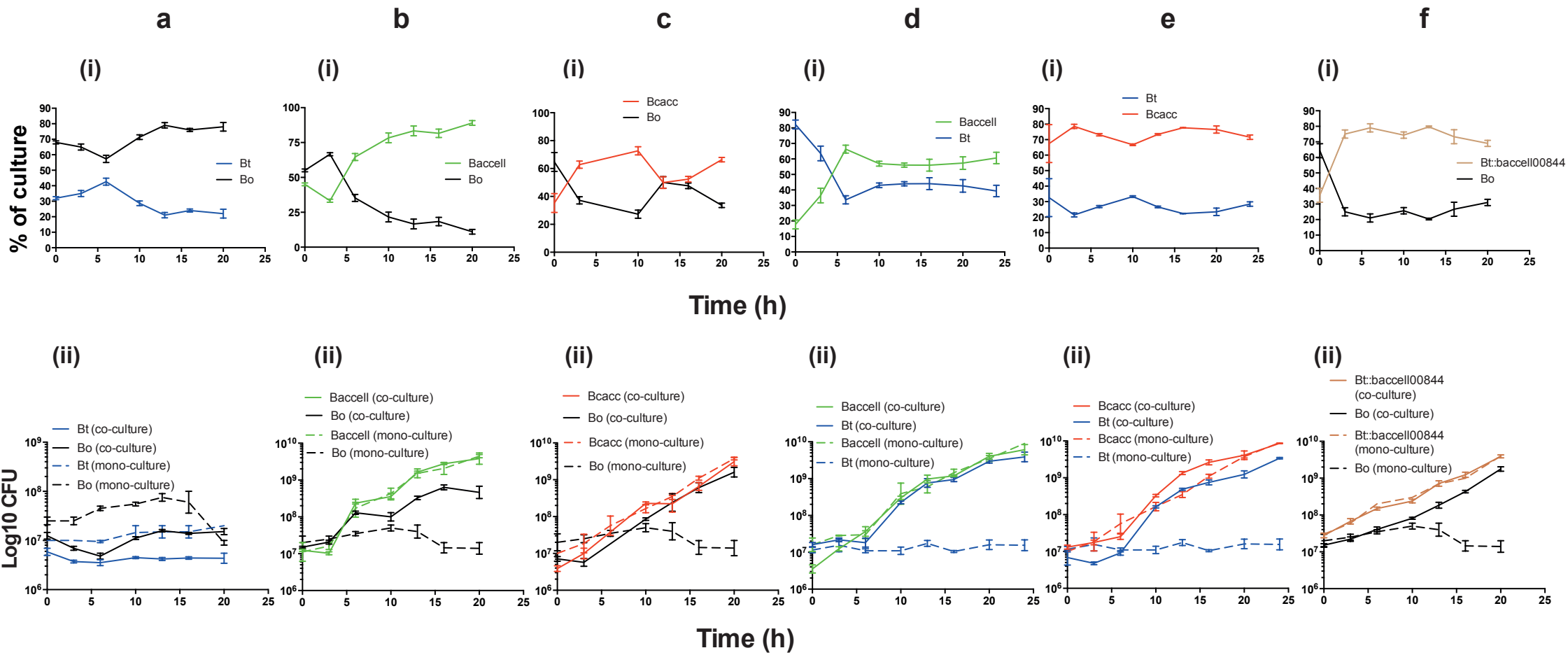


**Fig. 6**